CENTER FOR TRANSPORTATION INFRASTRUCTURE AND SAFETY

Structural Assessment of Highway "N" Power Substation under Earthquake Loads

by

Genda Chen, Ph.D., P.E.
Dongming Yan, Ph.D.
Zuocai Wang, Ph.D. Candidate
Seth Justin McConnell
David Rogers, Ph.D., R.G.
Kazi R. Karim, Ph.D.

A National University Transportation Center at Missouri University of Science and Technology

Disclaimer

The contents of this report reflect the views of the author(s), who are responsible for the facts and the accuracy of information presented herein. This document is disseminated under the sponsorship of the Department of Transportation, University Transportation Centers Program and the Center for Transportation Infrastructure and Safety NUTC program at the Missouri University of Science and Technology, in the interest of information exchange. The U.S. Government and Center for Transportation Infrastructure and Safety assumes no liability for the contents or use thereof.

Technical Report Documentation Page

1. Report No. NUTC R213 & R228	2. Government Accession No.	3. Recipient's Catalog No.
4. Title and Subtitle Structural Assessment of Highway "N" Power Substation under Earthquake Loads		5. Report Date October 2009 6. Performing Organization Code
7. Author/s Genda Chen, Dongming Yan, Zuocai Wang, Seth Justin McConnell, David Rogers and Kazi R. Karim		8. Performing Organization Report No. 00019054 & 00022574
9. Performing Organization Name and Address Center for Transportation Infrastructure and Safety/NUTC program Missouri University of Science and Technology 220 Engineering Research Lab Rolla, MO 65409		10. Work Unit No. (TRAIS) 11. Contract or Grant No. DTRT06-G-0014
12. Sponsoring Organization Name and Address U.S. Department of Transportation Research and Innovative Technology Administration 1200 New Jersey Avenue, SE Washington, DC 20590		13. Type of Report and Period Covered Final 14. Sponsoring Agency Code
15. Supplementary Notes		

16. Abstract

In this study, the Highway N Substation was analyzed with a finite element model (FEM) for its vulnerability. The ‘rigid’ bus and electric switch components were characterized with full scale shake table tests. Each component of the substation was carefully modeled with due considerations of mass density, stiffness and geometries. Based on the FEM, modal analysis was conducted to identify the natural frequencies of the structure along with their corresponding mass participation factors. In response spectrum and time history analyses, the dynamic responses of main components, such as ‘rigid’ buses and switches, were evaluated. The magnitude and location of the maximum moments were identified. The shake table tests on three Turner Electric’s TMX switches indicated that the first three natural frequencies of the switches are approximately 7.41 Hz, 15.2 Hz and 22.9 Hz, respectively. They are significantly higher than their corresponding frequencies of the entire substation system. The tested switches consistently fractured at the base of their metal shaft, a critical component of the switch open-and-close mechanism, due to stress concentration and local manufacture defect.

17. Key Words Power substation, finite element model, modal analysis, response spectrum analysis, time history analysis, shake table test	18. Distribution Statement No restrictions. This document is available to the public through the National Technical Information Service, Springfield, Virginia 22161.		
19. Security Classification (of this report) unclassified	20. Security Classification (of this page) unclassified	21. No. Of Pages 55	22. Price

Form DOT F 1700.7 (8-72)

RESEARCH INVESTIGATION

NUMERIAL AND EXPERIMENTAL STUDY ON SEISMIC VULNERABILITY OF THE HIGHWAY N SUBSTATION

PREPARED FOR

AMEREN CORPORATION

INCOLLABORATION WITH THE CENTER FOR TRANSPORTATION

INFRASTRUCTURE AND SAFETY AT MISSOURI UNIVERSITY OF SCIENCE

AND TECHNOLOGY

Written by:
Genda Chen, Ph.D., P.E.
Dongming Yan, Ph.D.
Zuocai Wang, Ph.D. Candidate
Seth Justin McConnell
David Rogers, Ph.D., R.G.
Kazi R. Karim, Ph.D.

CENTER FOR INFRASTRUCTURE ENGINEERING STUDIES
MISSOURI UNIVERSITY OF SCIENCE AND TECHNOLOGY

Submitted
October 16, 2009

The opinions, findings and conclusions expressed in this report are those of the principal investigators only. This report does not constitute a standard, specification or regulation.

TABLE OF CONTENTS

LIST OF FIGURES v
LIST OF TABLES vii
NOTATIONS viii
1 INTRODUCTION 1
2 FINITE ELEMENT MODEL OF THE HIGHWAY N SUBSTATION 3
3 MODAL ANALYSIS 4
3.1 Classical modal analysis theory 4
3.2 Modal analysis of the electrical substation 5
4 RESPONSE SPECTRUM ANALYSIS 10
4.1 Response spectrum 10
4.2 Response spectrum analysis 11
5 TIME HISTORY ANALYSIS 15
5.1 Spectrum compatible ground motions 15
5.2 Site-specific synthetic ground motion 22
6 SHAKE TABLE TEST OF SWITCHES 27
6.1 Test setup and instrumentation 28
6.2 Excitation and test procedure 31
6.3 Frequency transfer function estimates 31
6.4 Structural identification with force vibration tests 33
6.5 Structural identification with free vibration tests 36
6.6 Modal analysis of the specimen 36
6.7 Break tests 37
6.8 Time-varying frequency identification 39
7 REMARKS 42
ACKNOWLEDGEMENT 42
REFERENCES 43

LIST OF FIGURES

Figure 1 Typical damage resulting from earthquakes (Konagai, 2001) 2
Figure 2 FEM of the entire substation 3
Figure 3 FEM of the partial substation 3
Figure 4 The first 20 mode shapes 9
Figure 5 Response spectrum 10
Figure 6 Moment distribution along main buses 13
Figure 7 Illustration of moment distribution along main bus 2 13
Figure 8 The best matched response spectrum versus design spectrum 15
Figure 9 Time history of the synthetic ground motion 16
Figure 10 Moment envelop of main buses under the X-directional ground motion 17
Figure 11 Moment envelop of main buses under the Y-directional ground motion 18
Figure 12 Displacement time histories at joint A (-X side) under ground motions 19
Figure 13 Displacement time histories at joint A (+X side) under ground motions 20
Figure 14 Open-and-close of the switches under ground motions 21
Figure 15 Synthetic ground motions at the project site 23
Figure 16 Moment envelope under X-component of the M7.5 earthquake 25
Figure 17 Moment envelope under Y-component of the M7.5 earthquake 26
Figure 18 Dimensions of the shake table 27
Figure 19 Test setup and instrumentation of Turner TMX B104 vertical break switches .. 29
Figure 20 Wood truss system 30
Figure 21 Two data acquisition systems 30
Figure 22 Time history and Fourier transform 31
Figure 23 Relationship between excitation and response 32
Figure 24 Excitation and response of Switch No.2 33
Figure 25 FRF with an excitation frequency of 7.6 Hz: Switch No. 2 34
Figure 26 FRF at 7.8 Hz excitation frequency: Switch No.2 35
Figure 27 Free vibration of Switch No.2 36
Figure 28 FEM of the switch specimen 37
Figure 29 Mode shapes of the specimen 37
Figure 30 Break test results of Switch No.2 38
Figure 31 Break test results of Switch No.3 38

Figure 32 Failure mode of Switch No.3.. 39
Figure 33 Fundamental frequency and damping ratio identified of Switch No.3 40
Figure 34 Relative displacement and fundamental frequency identified over time 41

LIST OF TABLES

Table 1 Frequencies, periods and mass participating factors 6
Table 2 Parameters used in calculation of spectral response accelerations 10
Table 3 Relative acceleration, velocity and displacement 11
Table 4 Maximum moment in each bus (kip-in) 14
Table 5 Maximum moment in each bus (kip-in) 18
Table 6 Maximum moment under an M7.0 earthquake at 100 km distance (kip-in) 23
Table 7 Maximum moment under an M7.5 earthquake at 240 km distance (kip-in) 24
Table 8 Natural frequencies of Switch No. 2 35

NOTATIONS

c_r	Damping coefficient of the r^{th} mode of vibration
$F(\omega)$	Fourier transform of the measured excitation
$G_{fk}(\omega)$	Cross-correlation power spectrum density
$G_{ff}(\omega)$	Auto-correlation power spectrum density
$H(\omega)$	Frequency response function
$[K]$	Stiffness matrix of a structural system
k_r	Stiffness coefficient of the r^{th} mode of vibration
m_r	Mass coefficient of the r^{th} mode of vibration
$M(\omega)$	Noise in response measurement
$[M]$	Mass matrix of the structural system
N	Number of degrees of freedom
$N(\omega)$	Noise in excitation measurement
$\{P(t)\}$	External load vector
$q_r(t)$	r^{th} modal displacement
$\{q(t)\}$	Generalized displacement vector
u_i, u_j	Peak responses at time instances i and j
$\{U(t)\}$	Displacement vector
$X(\omega)$	Fourier transform of the measured response
$Y(\omega)$	Fourier transform of the actual response
$Z(\omega)$	Fourier transform of the actual excitation
$\{\phi_r\}$	r^{th} mode vector
$[\Phi]$	Collection of all mode vectors
ς	Damping ratio
ω	Excitation frequency
ω_r	r^{th} natural frequency

1 INTRODUCTION

History has repeatedly demonstrated that strong earthquakes occurred in urban areas. They often lead to devastating damage of constructed facilities, such as lifeline systems, gas and water distribution systems, power transmission systems and communication networks, threatening the safety and security of citizens and impacting regional economy. For example, the El Salvador Earthquake that occurred on January 13, 2001, Japan, caused nationwide damage to the electric power system with an estimated repair cost of more than $750,000 U.S. dollars (Konagai, 2001). To minimize losses such as these, shortly after an earthquake, damaged substations must be repaired and resumed to full operation. Typical damages were observed in transformers, bushings, interrupters, connectors, radiators, circuit breakers, surge arresters and capacitor banks. This highlights the need to identify and strengthen the critical components of these systems so that their functionality during future earthquakes is ensured.

A power substation is comprised of interconnected components including bushings, interrupters, connectors, radiators, circuit breakers and surge arresters. Some components of power substations such as porcelain insulators and bushings were quite susceptible to earthquakes and easily broken due to strong shaking. Typical damage caused during an earthquake is shown in **Figure 1**. These equipment items are usually connected to each other through conductor buses or flexible cables. In the event of earthquakes, these connections may induce dynamic interaction among the items. Previous studies (Kiureghian and Sackman et al., 1999; Kiureghian and Hong, 2000) have indicated that the dynamic characteristics may have contributed significantly to the damage of power substations. However, design guidelines or analysis methods that account for this interaction effect are currently unavailable.

(a) Broken bushing of a transformer **(b) Broken bushing of a lightning rod**

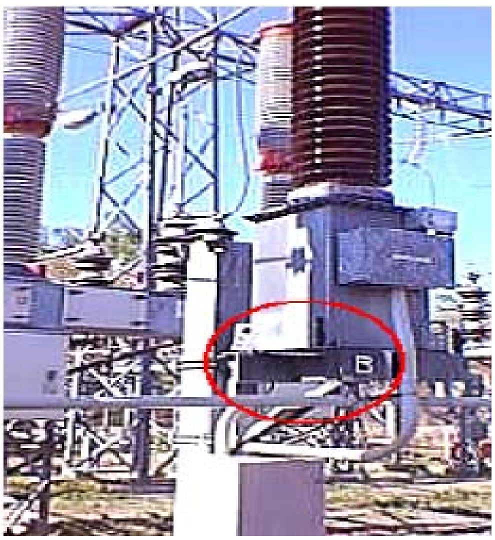

(c) Oil leakage from the bottom end of radiator **(d) Broken support of interrupter**

(e) Broken insulator

Figure 1 Typical damage resulting from earthquakes (Konagai, 2001)

2 FINITE ELEMENT MODEL OF THE HIGHWAY N SUBSTATION

This section describes the seismic performance evaluation of various components of the Highway N Substation using a site-specific design response spectrum or a synthesized ground motion for the region. The SAP2000 (CSI Inc. Version 10.0.9) finite element code was used to develop a model of the power substation. **Figure 2** shows the finite element model (FEM) of the main parts of the substation, including posts, porcelain bushings, rigid bus, dampers, and cables. Due to similar configurations among various parts of the structure, only part of the model as shown in **Figure 3** was used in various analyses. The upper rigid buses (4, 5, and 6) are oriented in 90° with the lower rigid buses (1, 2, and 3). The sliding mechanisms such as sleeves in the rigid bus and the electric switches were modeled by constraining two sets of nodes at the two sides of each sliding mechanism except for their slippage along the centerline of a rigid bus and a switch arm.

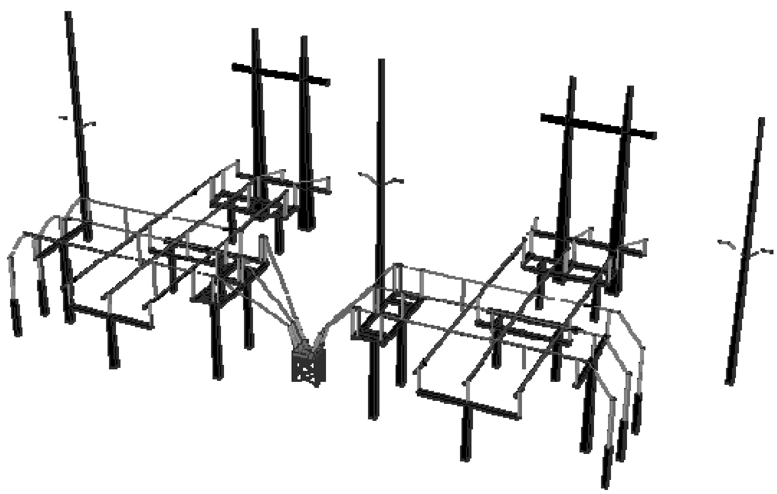

Figure 2 FEM of the entire substation

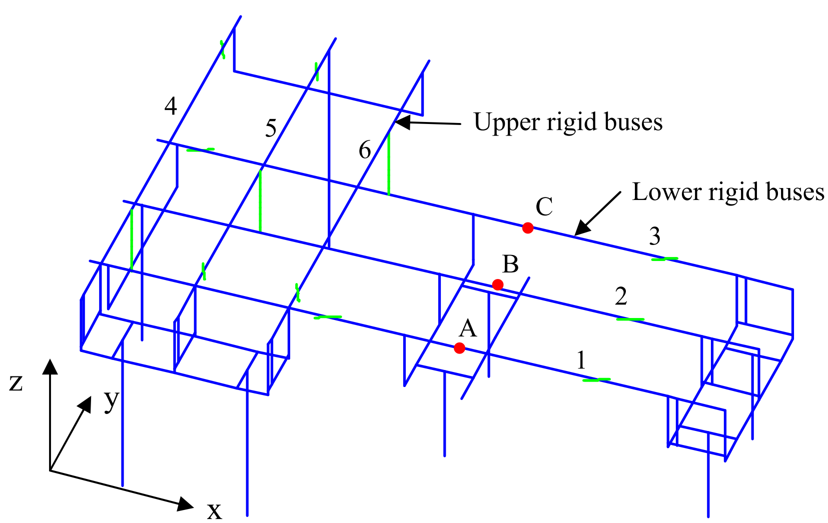

Figure 3 FEM of the partial substation

3 MODAL ANALYSIS

The modal analysis of the Highway N substructure was conducted to determine the natural frequencies and mode shapes of the structure and evaluate its responses under dynamic loading. In general, the dynamic responses of the structure are governed by a number of the lowest vibration modes.

3.1 Classical modal analysis theory

The equation of motion of a linear undamped multiple degree of freedom (MDF) system can be written as:

$$[M]\{\ddot{U}(t)\}+[K]\{U(t)\}=\{P(t)\} \tag{1}$$

in which $[M]$ and $[K]$ are the mass and stiffness matrices of the structural system, $\{U(t)\}$ is the displacement vector as a function of time, t, and $\{P(t)\}$ is the external load vector.

The displacement vector $\{U(t)\}$ of an MDF system can be expanded into a summation of modal contributions. That is,

$$\{U(t)\}=\sum_{r=1}^{N}\{\phi_r\}q_r(t)=[\Phi]\{q(t)\} \tag{2}$$

where N is the number of degrees of freedom, $\{\phi_r\}$ is the r^{th} mode vector, $[\Phi]$ is a collection of all mode vectors, $q_r(t)$ is the r^{th} modal displacement, and $\{q(t)\}$ is a generalized displacement vector or a collection of modal displacement. By using Eq. (2), the coupled equation (1) in $\{U(t)\}$ can be transformed to a set of uncoupled equations with the unknown modal displacement $q_n(t)$ after modal orthogonality conditions have been introduced (Chopra 2006). That is,

$$m_n\ddot{q}_n(t)+k_nq_n(t)=p_n(t) \tag{3}$$

in which $m_n=\{\phi_n\}^T[M]\{\phi_n\}$ and $k_n=\{\phi_n\}^T[K]\{\phi_n\}$ are the n$^{\text{th}}$ modal mass and stiffness, $p_n(t)=\{\phi_n\}^T\{P(t)\}$ is a n$^{\text{th}}$ modal force. Eq. (3) represents a generalized single degree of freedom (SDF) system. The natural frequency ω_n of the SDF system can be evaluated by:

$$\omega_n=\sqrt{\frac{k_n}{m_n}} \tag{4}$$

When damping is present, the n$^{\text{th}}$ modal equation of motion can be modified into

$$m_n \ddot{q}_n(t) + c_n \dot{q}_n + k_n q_n(t) = p_n(t) \tag{5}$$

where c_n is the damping coefficient of the nth mode of vibration. Eq. (5) indicates that the nth modal displacement $q_n(t)$ depends on its corresponding natural frequency ω_n, damping ratio $c_n / 2\sqrt{m_n k_n}$, and the frequency content of external excitations. After the modal displacement $q_n(t)$ has been determined, the contribution of the nth mode to the displacement $\{U(t)\}$ can be evaluated by Eq. (2).

3.2 Modal analysis of the electrical substation

The natural frequencies and mode vectors of the structure were determined by an eigensolution method. For time-history analyses, the so-called Ritz-vector method was used since Ritz-vectors can converge to the response more rapidly than eigenvectors can (Wilson 1982). The Ritz vectors are generated by taking into account the spatial distribution of the dynamic loading, whereas the direct use of natural mode shapes neglects this very important information.

How many modes of vibration must be included in analysis is a practical question. In building design, a rule of thumb is that the accumulated modal participation mass factors in each horizontal direction must exceed 90%. For complex 3-D structures, it is usually difficult to achieve that level of mass participation in all directions. In this study, an effort was made to include an accumulated modal participation mass factor of over 90% in horizontal directions (X and Y directions in Figure 3). To this endeavor, a total of 40 modes are specified in the initial analysis of the structure to ensure satisfied accuracy of the first 20 vibration mode characteristics.

The natural frequencies of the first 20 modes with modal mass-participant factors are listed in Table 1 along with a brief description of each dominant motion and its respective modal participating mass ratio (MPMR). Here, the significant modes are defined as those with an MPMR of 2% or higher in any single direction. In Table 1, UX, UY, and UZ represent the translational motions along X, Y, and Z axes while RX, RY, and RZ, denote the rotational motions about X, Y, and Z axes, respectively. The MPMR value provides a measure of how important a particular mode of vibration is for the overall response to the acceleration loads in each of the three global directions though a small MPMR value could correspond to a significant local vibration mode. It helps ensure a significant and required number of vibration modes are included in the seismic response analysis. From **Table 1** it can be seen that the accumulated MPMR exceeds 90% in X and Y directions as well as in rotational motions about the vertical axis. The MPMR in vertical direction is low since the critical components, rigid buses, participated in various vibration are relatively light in comparison with vertical members. The fact that a less mass participation is observed in the vertical direction is likely attributable to the presence of flexible cables in the structure, where some of them vibrate independently of the remaining structure.

Table 1 Frequencies, periods and mass participating factors

Mode No.	Period (sec)	Frequency (Hz)	Mass participation factor (%)						Description
			UX	UY	UZ	RX	RY	RZ	
1	0.826	1.21	**7.5**	**1.6**	0.0	0.3	**4.3**	**11.9**	**UX+RY+RZ**
2	0.784	1.28	**25.7**	0.0	0.1	0.1	**3.5**	**18.0**	**UX+RY+RZ**
3	0.719	1.39	0.3	**44.5**	0.0	**12.2**	0.1	0.3	**UY+RX**
4	0.615	1.63	**32.5**	0.0	0.0	0.0	**12.6**	**4.7**	**UX+RY+RZ**
5	0.484	2.07	0.0	0.5	0.0	0.1	0.0	0.1	
6	0.410	2.44	0.0	0.3	0.0	0.0	0.0	0.2	
7	0.322	3.10	0.0	**32.3**	0.0	**3.6**	0.0	**34.1**	**UY+ RZ**
8	0.305	3.28	0.2	0.0	0.0	0.0	0.0	**2.1**	**RZ**
9	0.286	3.49	**25.3**	0.0	0.2	0.2	**3.2**	**17.4**	**UX+RY+RZ**
10	0.270	3.71	**1.1**	0.1	0.0	0.1	0.0	**2.0**	**RZ**
11	0.243	4.12	0.0	**12.6**	0.0	**1.3**	0.0	**1.9**	**UY+RZ**
12	0.233	4.29	0.4	0.0	0.0	0.0	0.0	0.3	
13	0.213	4.70	0.2	0.0	0.0	0.0	0.0	0.4	
14	0.204	4.90	0.0	**2.4**	0.1	0.2	0.0	0.0	**UY**
15	0.188	5.31	0.0	**4.3**	0.0	0.2	0.0	0.3	**UY**
16	0.180	5.55	0.0	0.1	0.1	0.1	0.0	0.0	
17	0.159	6.31	0.0	0.1	0.1	0.2	0.0	0.8	
18	0.147	6.79	0.3	0.0	**6.6**	**6.3**	0.3	0.2	**UZ+RX**
19	0.144	6.96	0.9	0.0	0.4	0.4	**3.6**	0.7	**RY**
20	0.141	7.08	0.3	0.0	**2.0**	**1.8**	0.4	0.2	**UZ+RX**
Total	-	-	94.7	99.0	9.6	27.3	28.1	95.6	

The first 20 mode shapes of vibration are presented in **Figure 4**. It can be seen that most modes correspond to the coupled motion in X and Y directions. This observation indicates that the structure is flexible in the X and Y direction. Indeed, the fundamental period of 0.826s mainly corresponds to the X movement of the tall part of the structure together with the slight Y movement and the rotation around Y and Z, as shown in **Figure 4**(a).

Figure 4(b) shows the second mode of vibration in the X direction at a period of 0.784 sec. The shape of the 3rd mode is shown in **Figure 4**(c); it mainly corresponds to the Y motion. The shapes of the 4th mode and 9th mode primarily correspond to the X motion while Modes 7, 11, 14 and 15 mainly correspond to the Y motion. Basically, the first 11 modes dominate the horizontal vibration of the substation structure. These modes are mainly related to the motion of the supports in the structure. After the 11th mode, more and more cables begin to participate in the motion. That is why the mass participant factors are relatively small for the several last vibration modes.

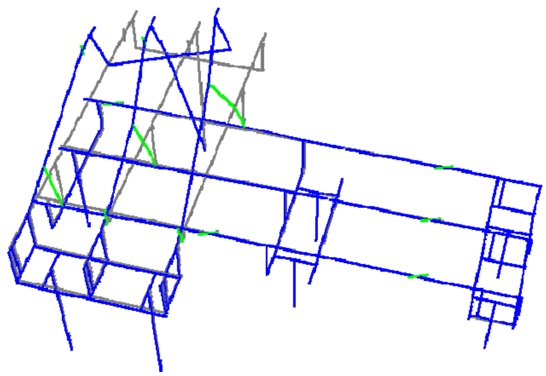

(a) Mode No. 1 (0.826 sec)

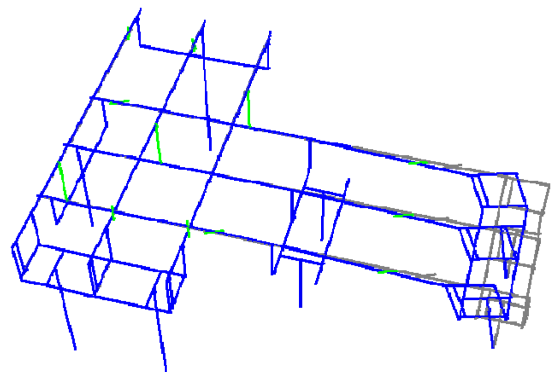

(b) Mode No. 2 (0.784 sec)

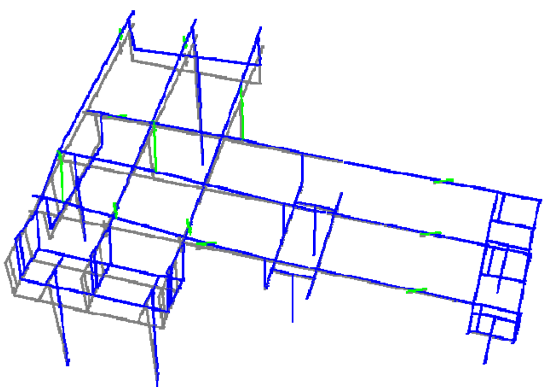

(c) Mode No. 3 (0.719 sec)

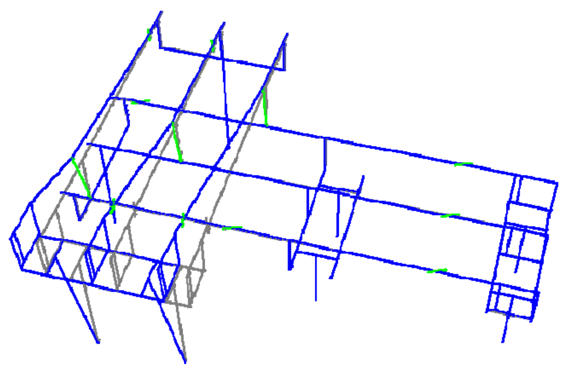

(d) Mode No. 4 (0.615 sec)

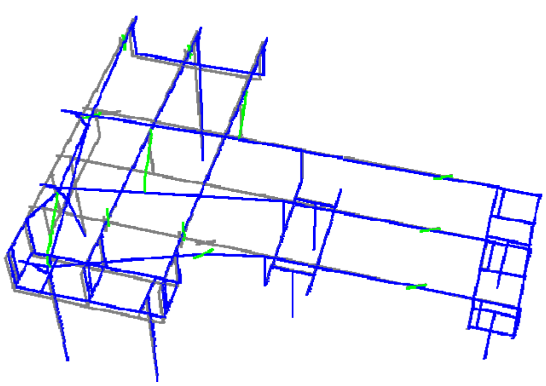

(e) Mode No. 5 (0.484 sec)

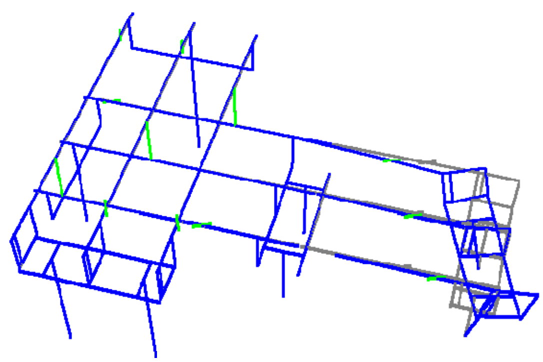

(f) Mode No. 6 (0.410 sec)

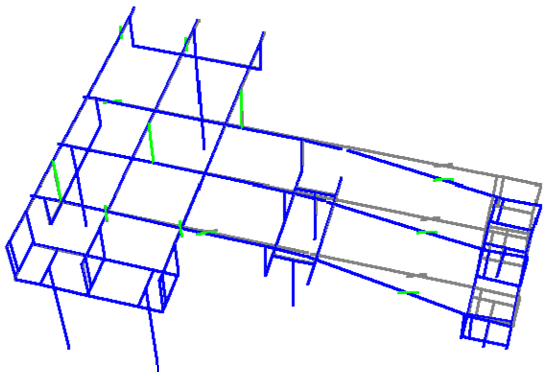

(g) Mode No. 7 (0.322 sec)

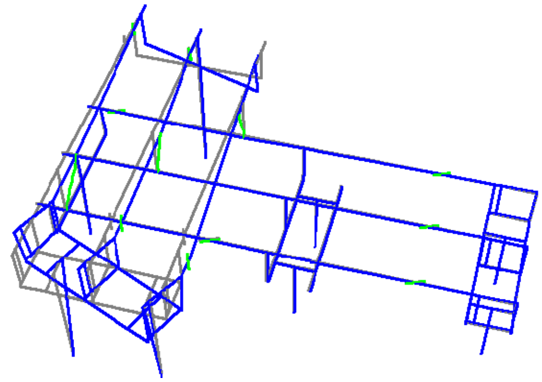

(h) Mode No. 8 (0.305 sec)

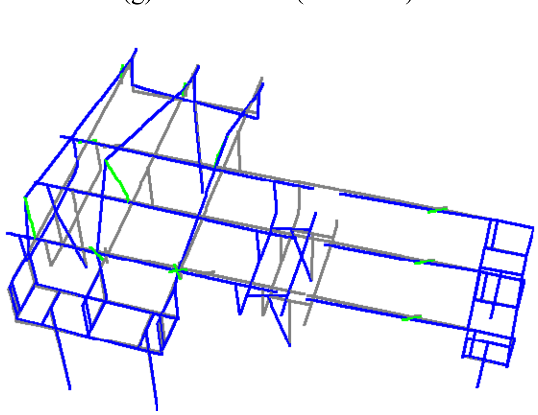

(i) Mode No. 9 (0.286 sec)

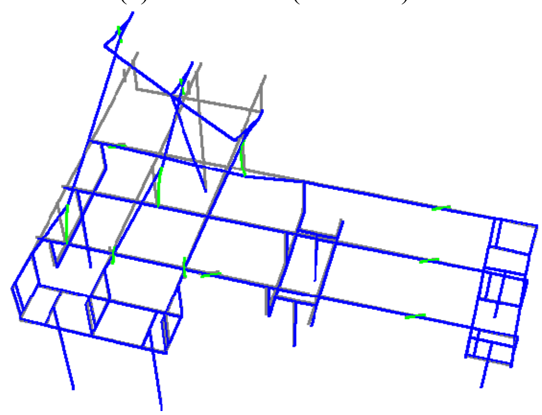

(j) Mode No. 10 (0.270 sec)

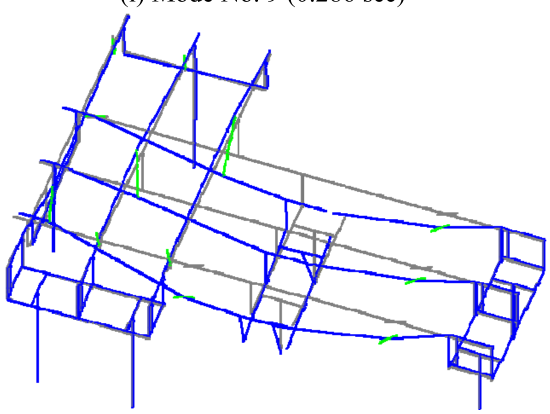

(k) Mode No. 11 (0.243 sec)

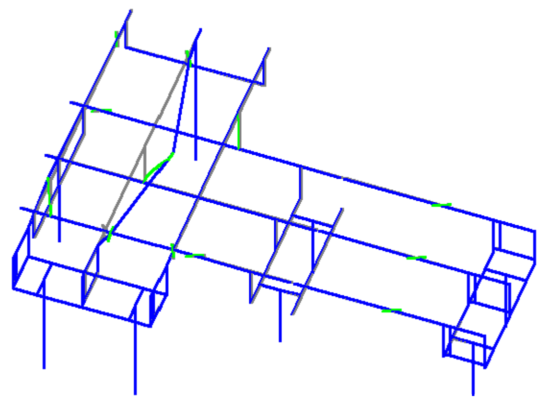

(l) Mode No. 12 (0.233 sec)

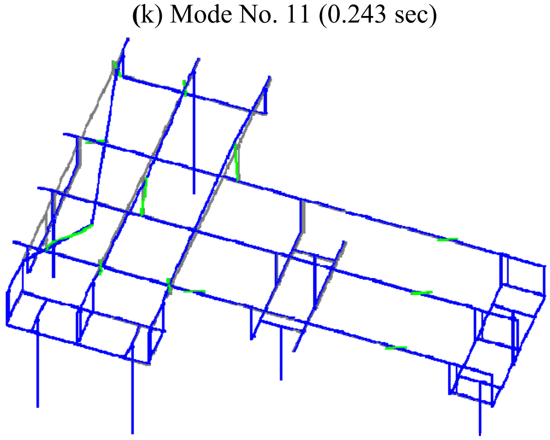

(m) Mode No. 13 (0.213 sec)

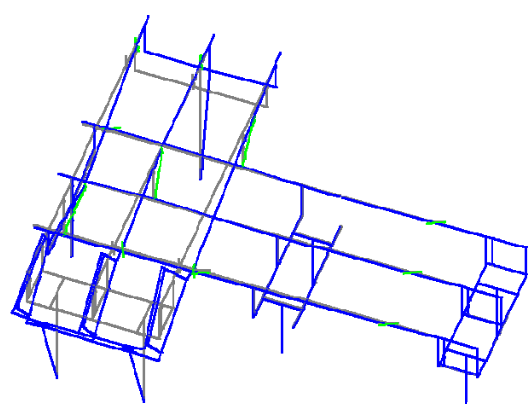

(n) Mode No. 14 (0.204 sec)

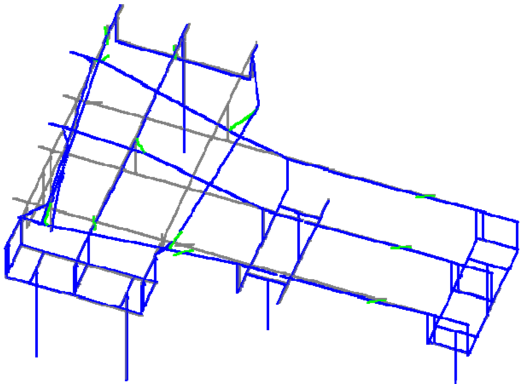
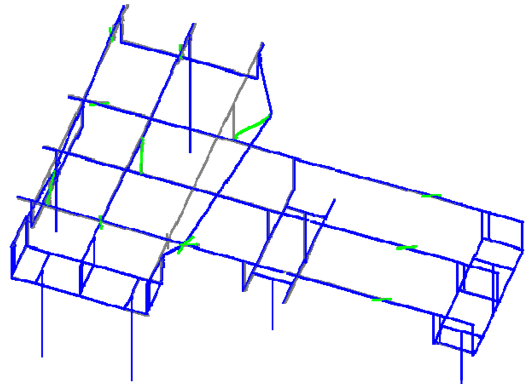

(o) Mode No. 15 (0.188 sec)

(p) Mode No. 16 (0.180 sec)

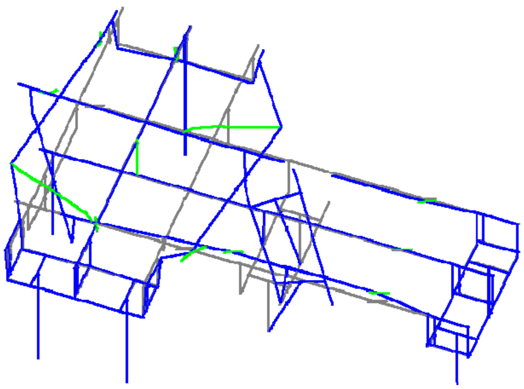
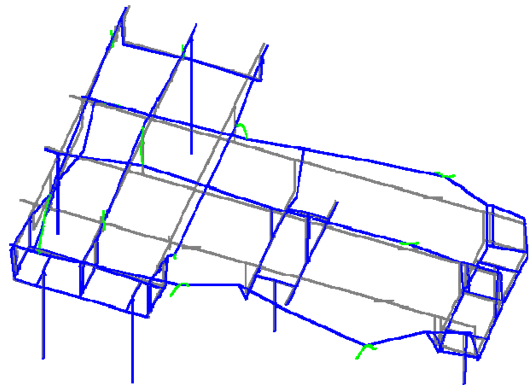

(q) Mode No. 17 (0.159 sec)

(r) Mode No. 18 (0.147 sec)

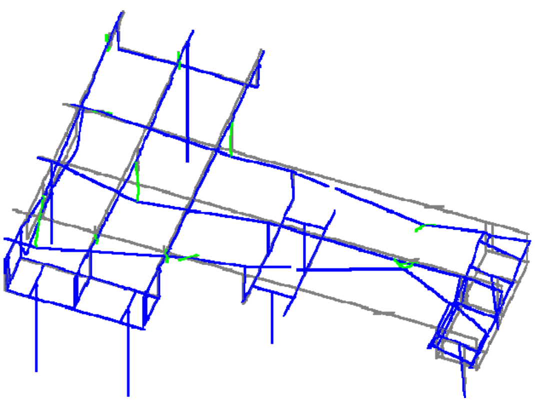
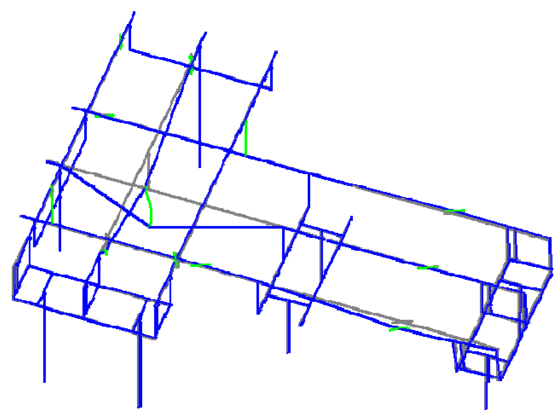

(s) Mode No. 19 (0. 144 sec)

(t) Mode No. 20 (0. 141 sec)

Figure 4 The first 20 mode shapes

4 RESPONSE SPECTRUM ANALYSIS

4.1 Response spectrum

The subsurface exploration at the project site was reported by Geotechnology (2004). Based on the soil condition, the project site was classified as Class D (IBC, 2003). In this case, the design spectral response accelerations (S_{DS} & S_{D1}) were calculated using the procedures outlined in Section 1615 of the 2003 IBC. Parameters used for estimation of the accelerations at short period (S_{DS}) and at one second period (S_{D1}) are presented in **Table 2**. The design response spectrum and the first five natural periods of the power substation structure are depicted in **Figure 5**.

Table 2 Parameters used in calculation of spectral response accelerations

"Soil Site Class D" where $1000 \leq s_u \leq 2000$ psf and $600 \leq Vs \leq 1200$ ft/sec	
The mapped spectral acceleration at short period	$Ss = 0.45$
The mapped spectral accelerations at one-second period	$S_1 = 0.15$
Site coefficient defined in Table 1642.1.2 (1) of 2003 IBC	$F_a = 1.4$
Site coefficient defined in Table 1642.1.2 (2) of 2003 IBC	$F_v = 2$
The design spectral response acceleration at short period	$S_{DS}= 0.42$
The design spectral response acceleration at one second period	$S_{D1}= 0.2$
Period of S_{DS}	$T_0 = 0.1$

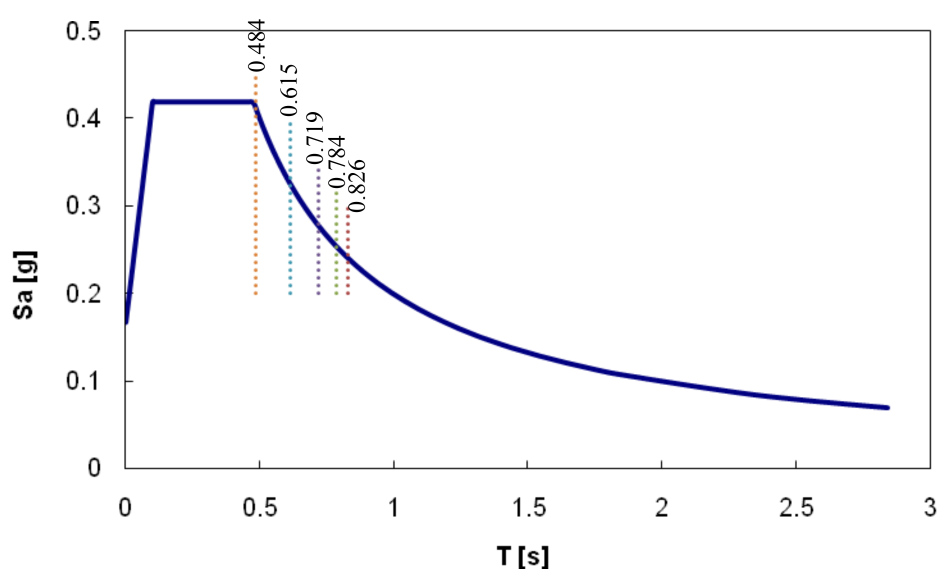

Figure 5 Response spectrum

4.2 Response spectrum analysis

The FEM of the power substation structure was analyzed under the design earthquake described by the response spectrum in **Figure 5**. The maximum relative velocity and displacement obtained at the three key points indicated in Figure 3 are listed in **Table 3**. The maximum relative displacements are approximately 2.24 inches.

Table 3 Relative acceleration, velocity and displacement

Location	Relative velocity (in/sec)	Relative displacement (in)
A	15.3	2.24
B	15.2	2.22
C	15.3	2.23

The flexural moment distributed along the six main buses are presented in

Figure 6. **Figure 6**(a, b) are due to the earthquake excitation in X direction while **Figure 6**(c, d) result from the excitation in Y direction. It is evidenced that the maximum out-of-plane moment occurred in lower main buses (1, 2, and 3) as a result of the Y-directional earthquake. The maximum in-plane moment occurs in upper main buses (4, 5, and 6) due to the X-directional earthquake.

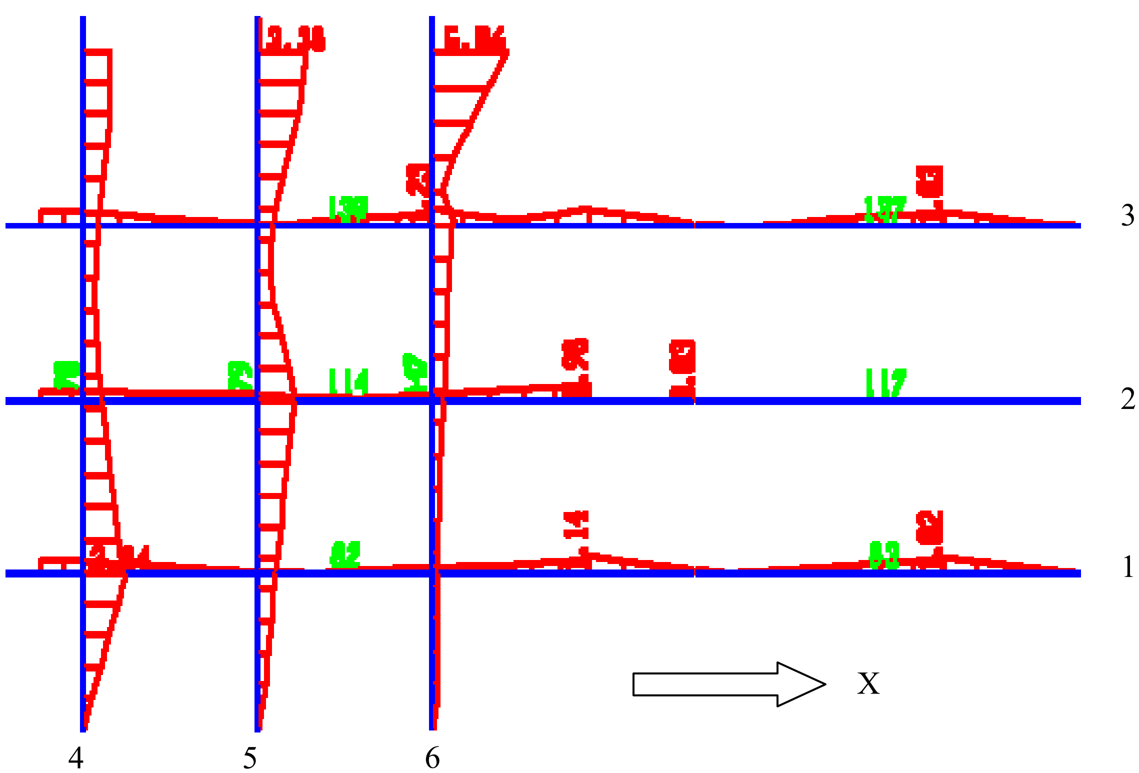

(a) Out-of-plane moment about vertical axis under X-directional earthquake

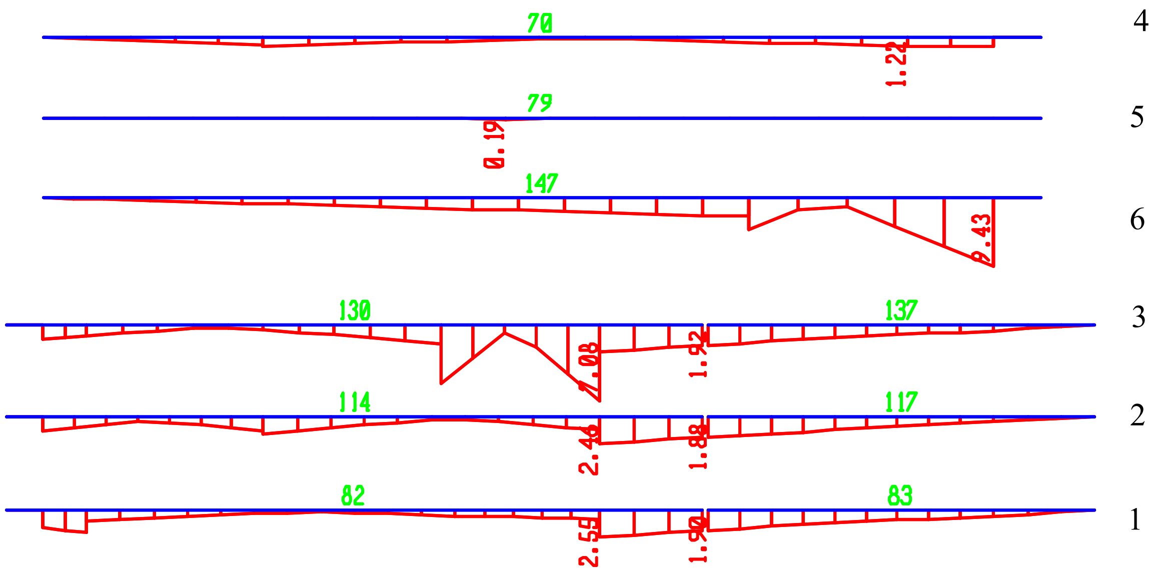

(b) In-plane moment about horizontal axis under the X-directional earthquake

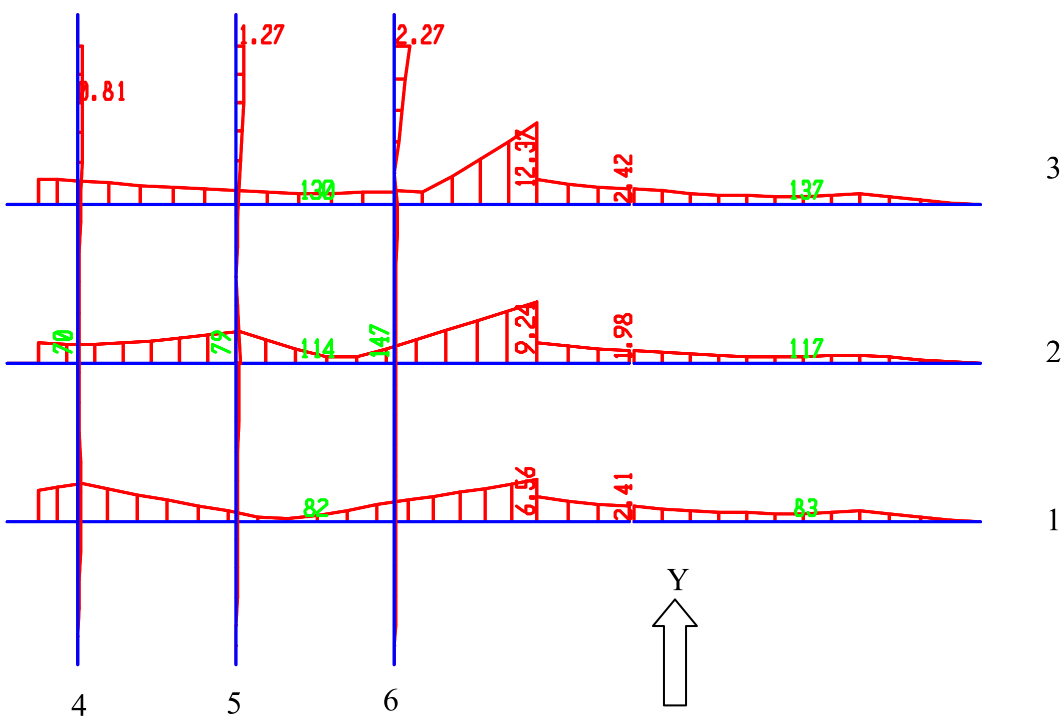

(c) Out-of-plane moment about vertical axis under the Y-directional earthquake

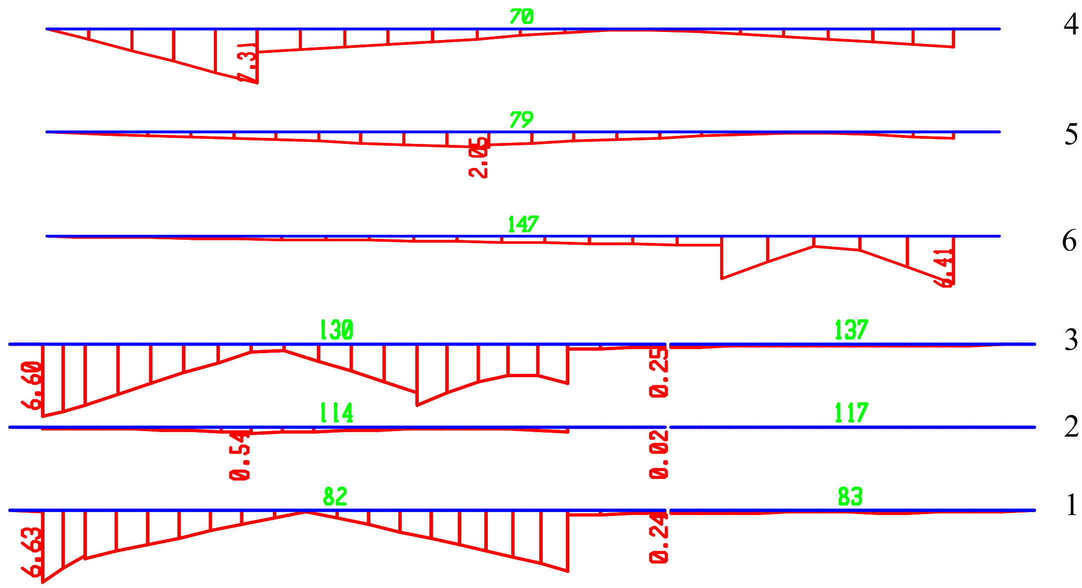

(d) In-plane moment under horizontal axis due to Y-directional earthquake

Figure 6 Moment distribution along main buses

Each main bus has at least one vibration absorber and a cable constraint between two levels of switch structures. **Figure 7** re-produces the in-plane moment distribution along the middle main bus at the lower level. Its variation is dominated by supporting conditions. For example, the main bus is constrained by the upper main bus through a vertical cable at point b, subjected to a shock absorber at point d, and supported by porcelain insulators at points a, c, and e.

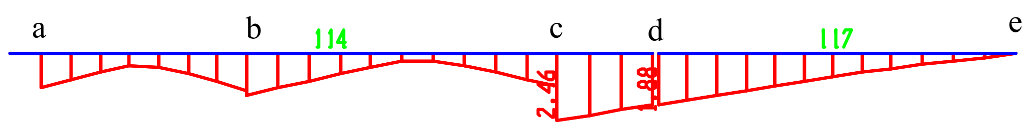

Figure 7 Illustration of moment distribution along main bus 2

It can be seen from

Figure 6 that the maximum moment in various buses varies. The absolute maximum moment among all the buses occurs in bus #3. It is noted that the larger value of vertical and transverse moments does not necessarily happen in the same direction. This observation can be seen in **Table 4**. The maximum moment in bus 3 reaches about 12.4 kip-in out of plan due to the Y-directional earthquake. It is also observed that both the 30% and the square-root-of-the-sum-of-the-squared load combination rules give higher moments due to the combined effect of directional earthquake components.

Table 4 Maximum moment in each bus (kip-in)

Earthquake component	Moment	Bus #1	Bus #2	Bus #3	Bus #4	Bus #5	Bus #6
X	In-plane	1.14	0.98	1.23	2.84	3.38	5.06
	Out-of-plane	2.55	2.46	7.08	1.22	0.19	**9.43**
Y	In-plane	6.56	9.25	**12.4**	0.81	1.27	2.27
	Out-of-plane	6.63	0.54	6.60	7.31	2.05	6.41
X + 30%Y	In-plane	3.11	3.76	4.94	3.08	3.76	5.74
	Out-of-plane	4.54	2.62	9.06	3.41	0.81	**11.4**
30%X + Y	In-plane	6.90	9.54	**12.7**	1.66	2.28	3.79
	Out-of-plane	7.40	1.28	8.72	7.68	2.11	9.24
$\sqrt{X^2 + Y^2}$	In-plane	6.66	9.30	**12.4**	2.95	3.61	5.55
	Out-of-plane	7.10	2.52	9.68	7.41	2.06	**11.4**

5 TIME HISTORY ANALYSIS

Two methods were employed to generate synthetic ground motions in this study. The first method is for the ground motions compatible with the design response spectrum as specified in the 2003 IBC. The second one is for site-specific ground motions generated with the point source model.

5.1 Spectrum compatible ground motions

Ground motions were generated to ensure their acceleration response spectrum compatible with that in **Figure 5**, taken from the 2003 IBC. First, 10 synthetic ground motions were generated to match the spectral accelerations, S_{DS} and S_{D1}. Their response spectra were then evaluated and compared with the design acceleration spectrum. The best matched spectrum is selected as illustrated in **Figure 8Error! Reference source not found.** along with the design spectrum. Its corresponding time history is presented in **Figure 9**. It is observed from **Figure 8** that the synthetic ground motion results in a response spectrum that matches well with the design spectrum. The design spectrum took into account the effects of foundation and site condition.

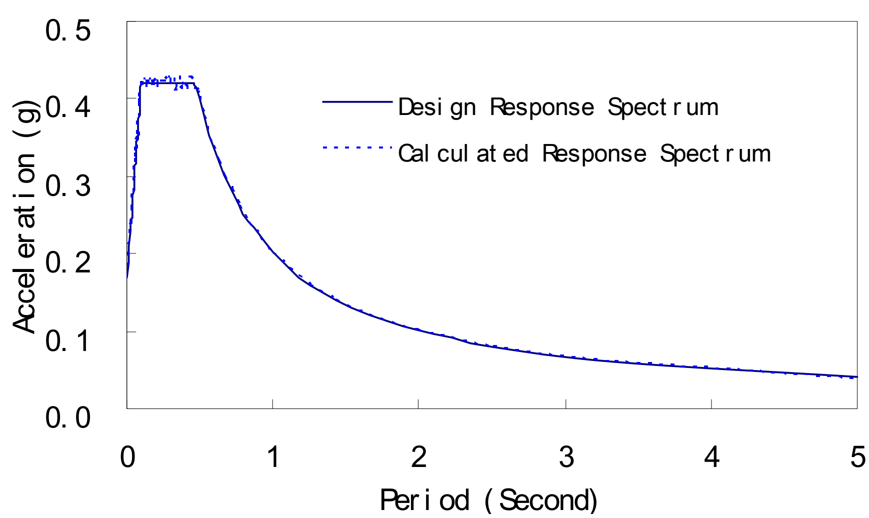

Figure 8 The best matched response spectrum versus design spectrum

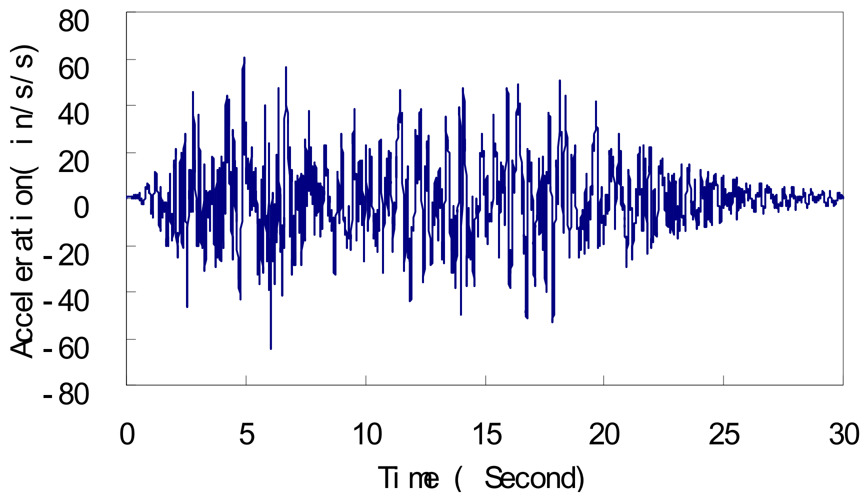

Figure 9 Time history of the synthetic ground motion

Time history analysis was also conducted with the FEM of the substation. All ground supports of the substation are subjected to the generated ground motion. Modal damping taken in this study was 0.05. The maximum moment is distributed along each bus as shown in **Figure** and **Figure 11** for out-of-plane and in-plane moments, respectively.

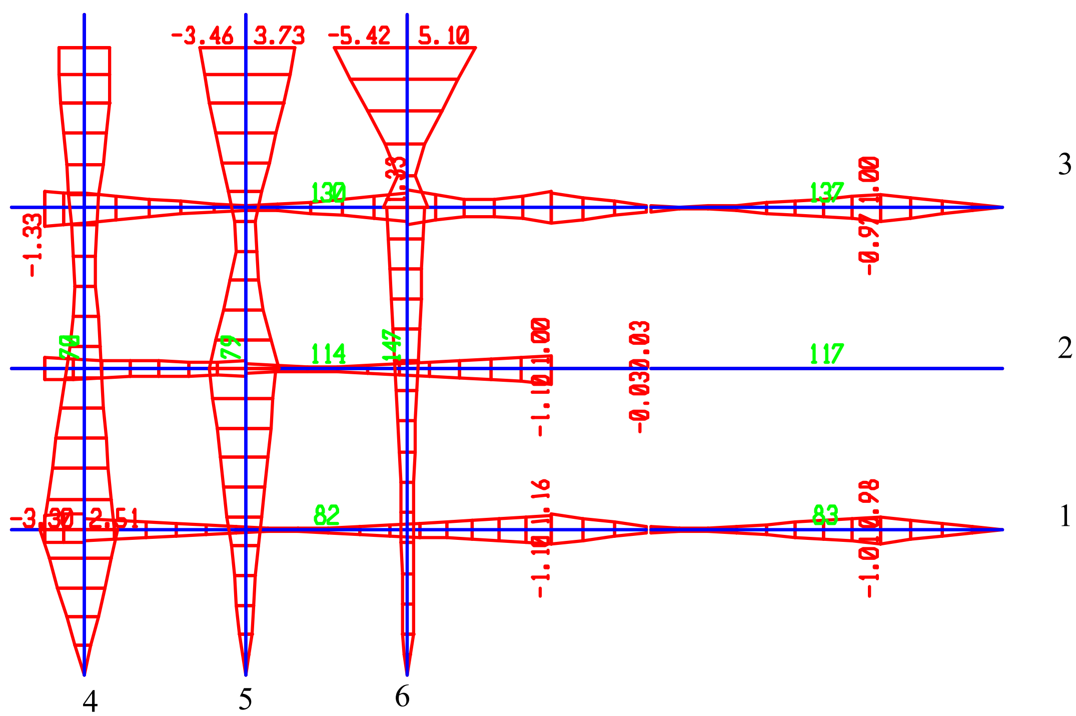

(a) Out-of-plane moment about the vertical axis

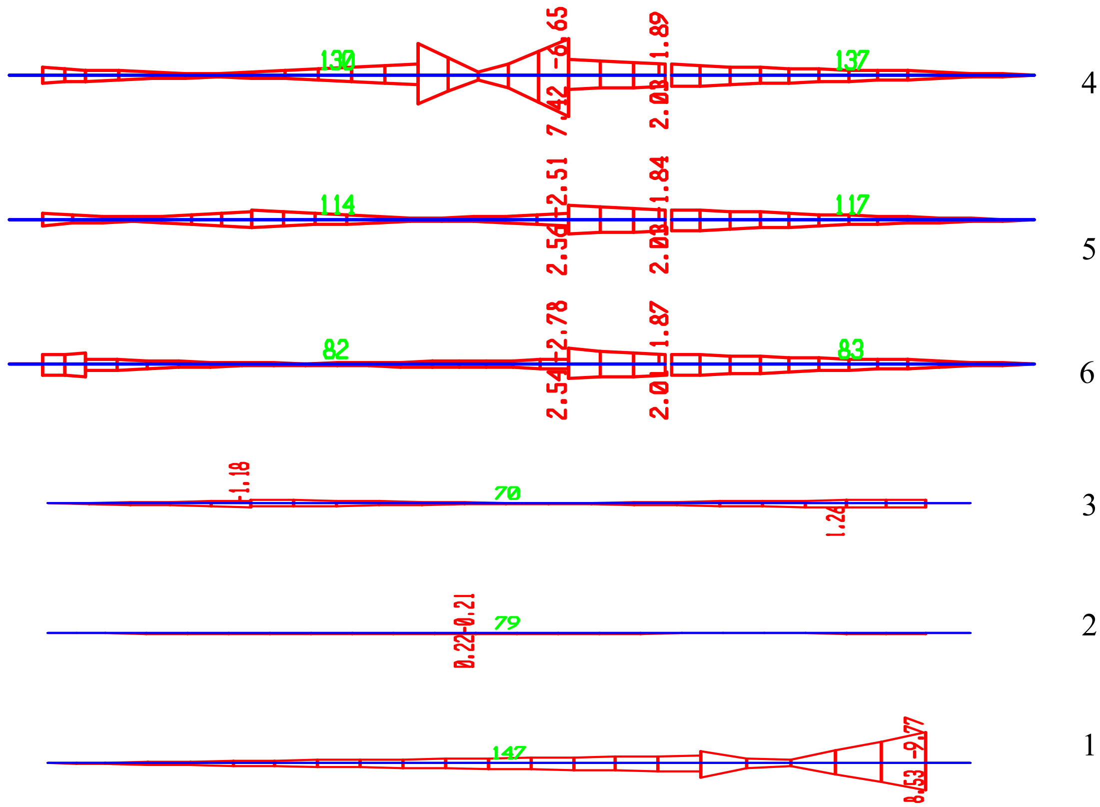

(b) In-plane moment about the horizontal axis

Figure 10 Moment envelop of main buses under the X-directional ground motion

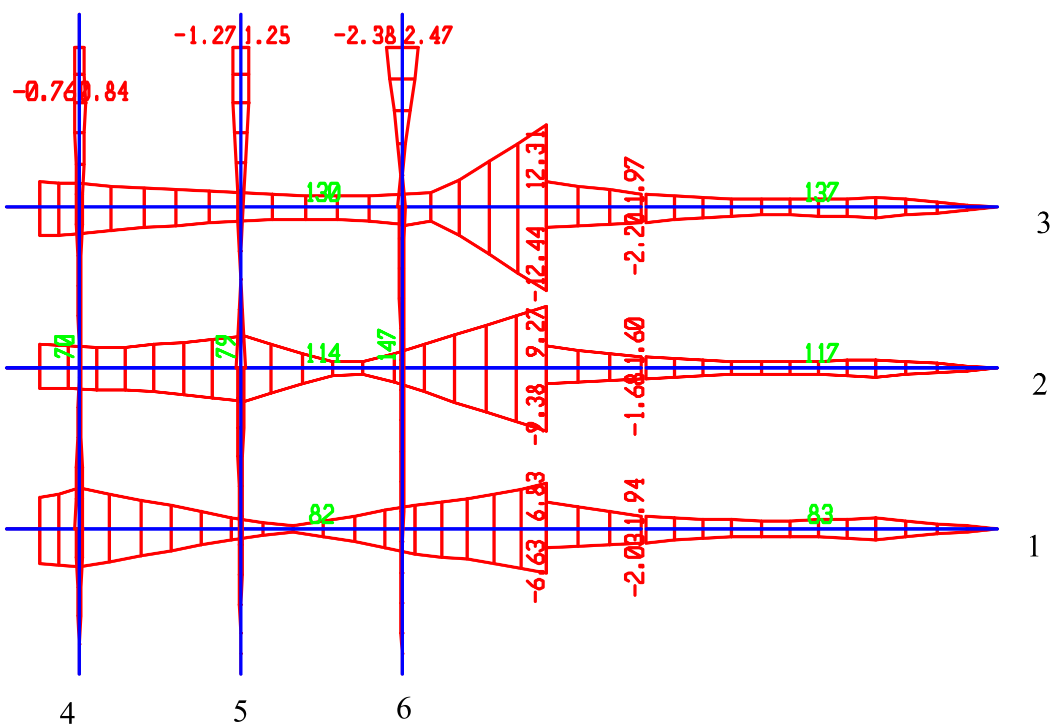

(a) Out of plane moment about the vertical axis

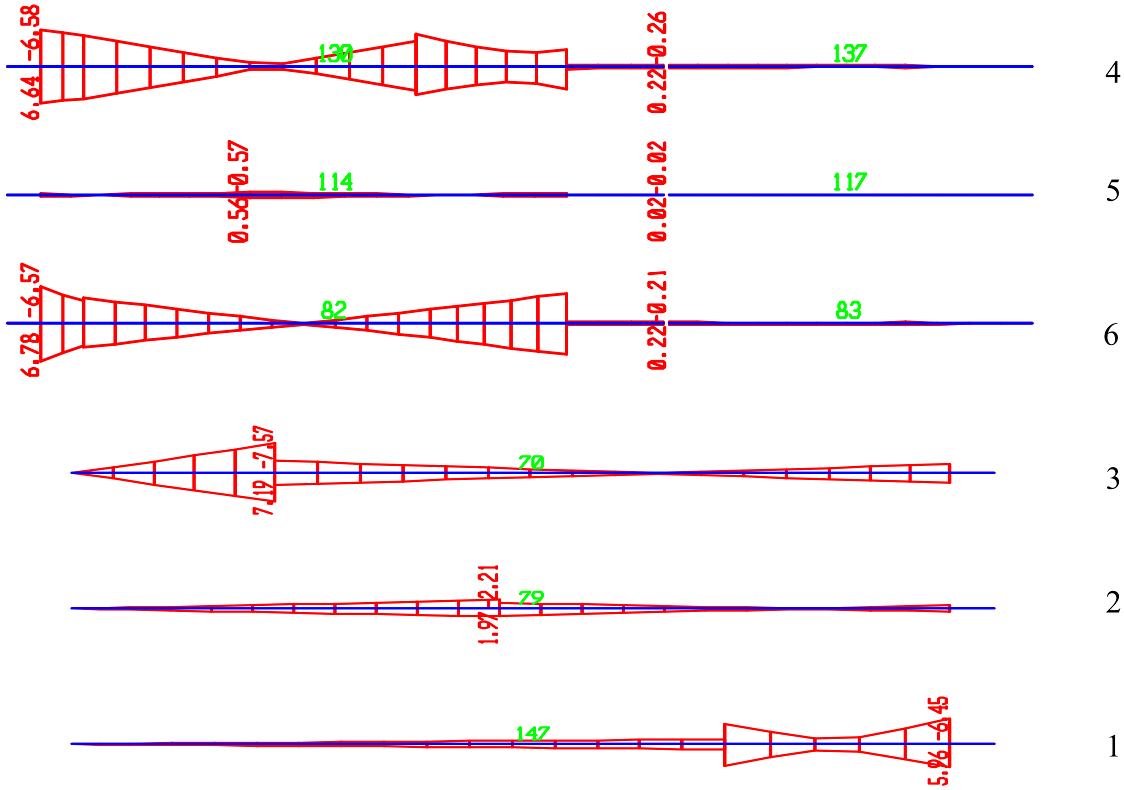

(b) In-plane moment around the horizontal axis

Figure 11 Moment envelop of main buses under the Y-directional ground motion

The maximum moments along each bus due to individual component earthquakes and their combination are summarized in **Table 5.** It can be seen from **Table 5** that the absolute maximum moments due to X- and Y-directional earthquakes are 9.77 kip-in and 12.4 kip-in, respectively. They occur in bus #6 and bus #3. Both the magnitude and location of the absolute moments well correspond to those from response spectrum analysis.

Table 5 Maximum moment in each bus (kip-in)

Earthquake component	Moment	Bus #1	Bus #2	Bus #3	Bus #4	Bus #5	Bus #6
X	In-plane	1.16	1.10	1.33	3.30	3.73	5.42
	Out-of-plane	2.78	2.56	7.42	1.26	0.22	**9.77**
Y	In-plane	6.83	9.38	**12.4**	0.84	1.27	2.47
	Out-of-plane	6.78	0.57	6.64	7.57	2.21	6.45
X + 30%Y	In-plane	3.21	3.91	5.06	3.55	4.11	6.16
	Out-of-plane	4.81	2.73	9.41	3.53	0.88	**11.7**
30%X + Y	In-plane	7.18	9.71	**12.8**	1.83	2.39	4.10
	Out-of-plane	7.61	1.34	8.87	7.95	2.28	9.38
$\sqrt{X^2+Y^2}$	In-plane	6.93	9.44	**12.5**	3.41	3.94	5.96
	Out-of-plane	7.33	2.62	9.96	7.67	2.22	**11.7**

The three-directional time history responses at joint "A" are presented in **Figure 12** and **Figure 13** under ground motions in X- and Y-direction, respectively. Since the main bus #1 with joint A is oriented along the X direction, the displacement at joint A (-X and +X sides) is the largest in the X- and Y-direction under the X- and Y-directional earthquakes, respectively. Note that U1, U2, and U3 in **Figures 12** and **13** represent the axial displacement and the transverse displacements both in horizontal and vertical directions.

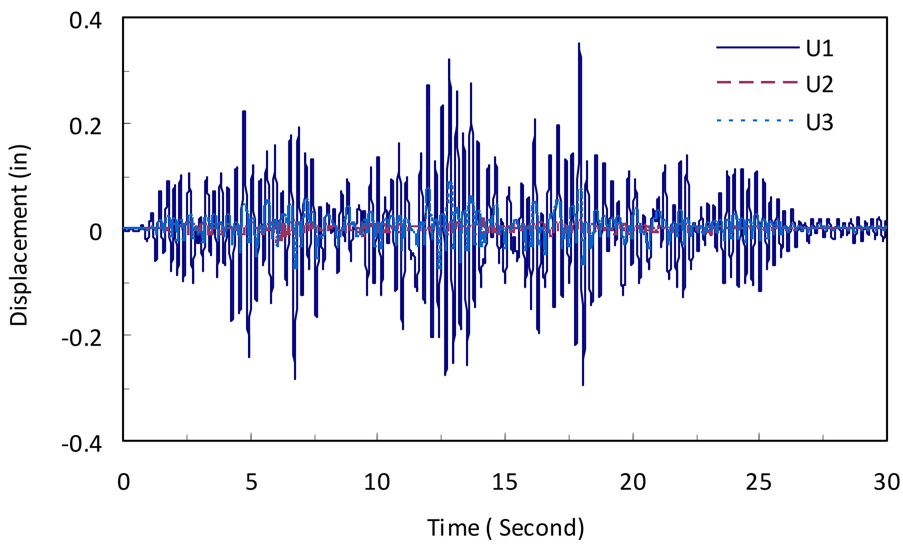

(a) Ground motion in X-direction

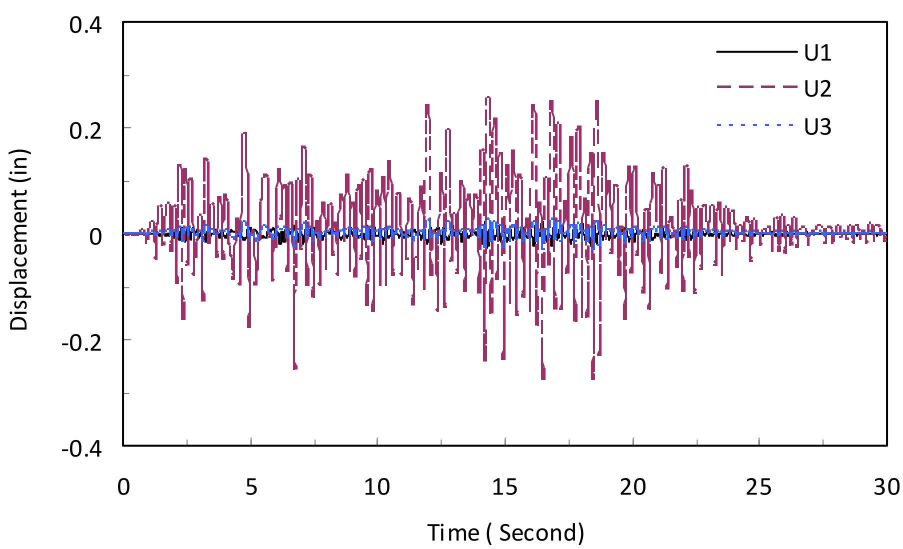

(b) Ground motion in Y-direction

Figure 12 Displacement time histories at joint A (-X side) under ground motions

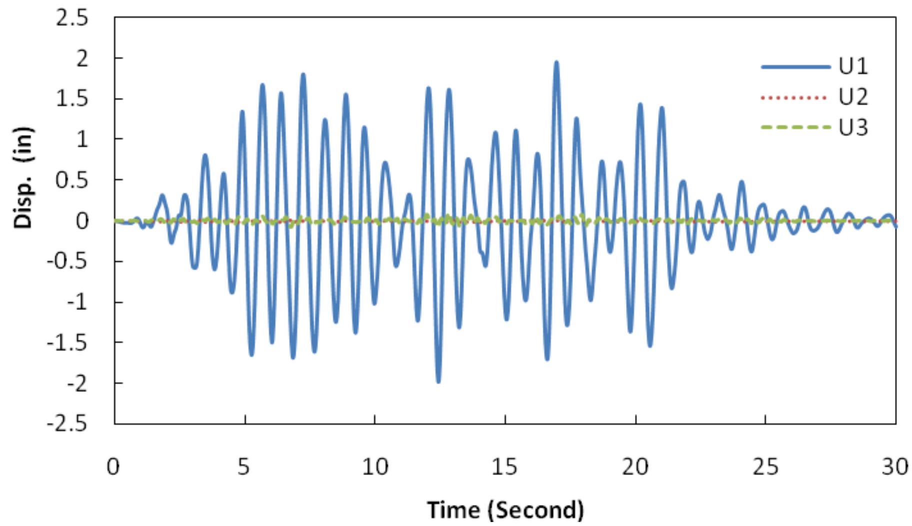

(a) Ground motion in X-direction

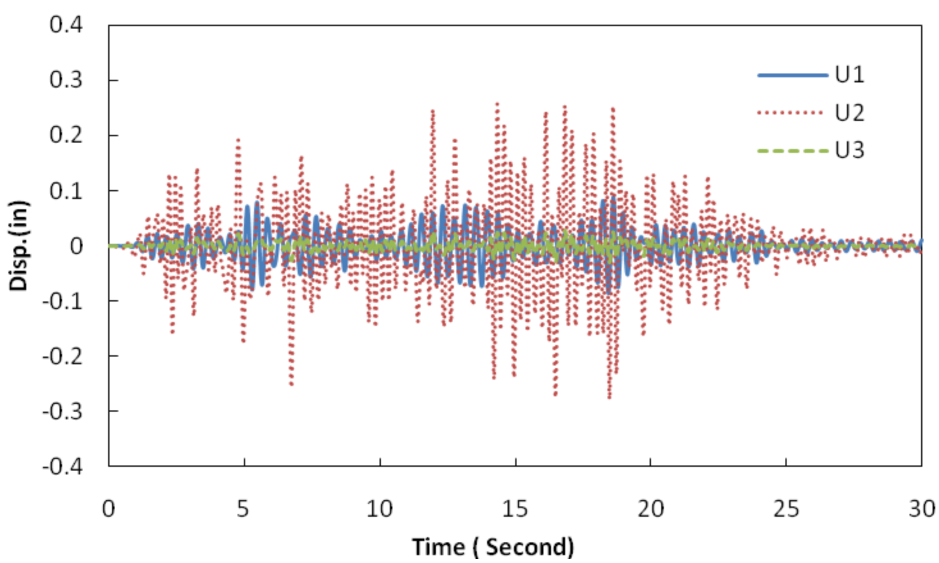

(b) Ground motion in Y direction

Figure 13 Displacement time histories at joint A (+X side) under ground motions

The relative displacements at three slip joints (A, B, and C) are presented in **Figure 14** as the difference between the motions on two sides of each joint. It can be seen from **Figure 14** that the maximum relative displacement reaches 1.86 inches, which is slightly less than that obtained from the response spectrum analysis. The dominant excitation is in the X- direction and the influence of the excitation from Y direction can be neglected.

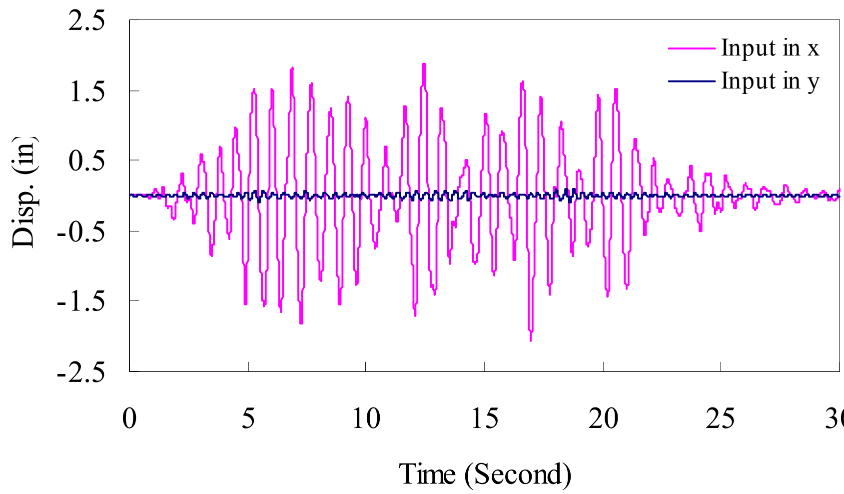

(a) Slip joint A

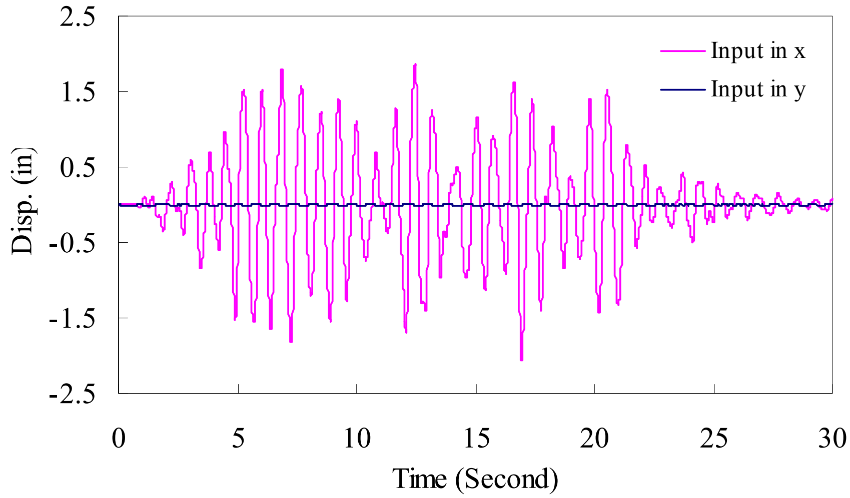

(b) Slip joint B

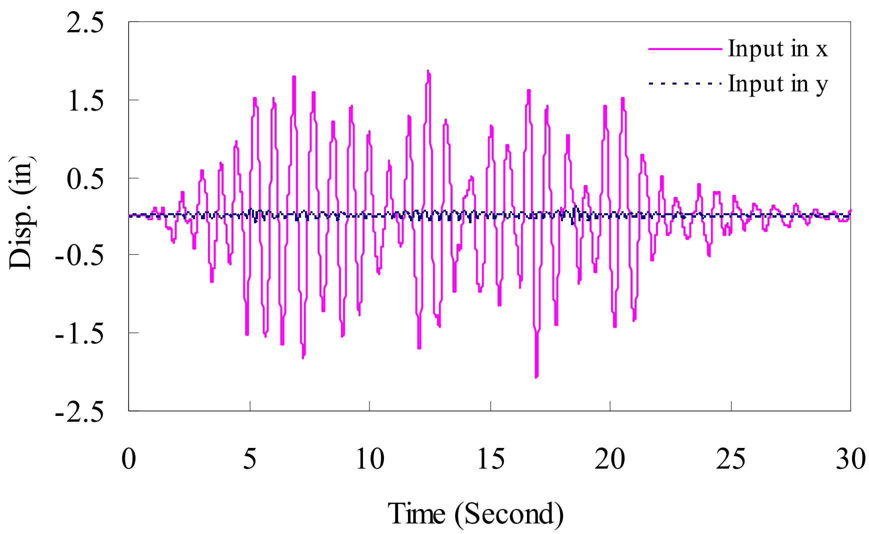

(c) Slip joint C

Figure 14 Open-and-close of the switches under ground motions

5.2 Site-specific synthetic ground motion

The epicenter distance and the earthquake magnitude were selected for the synthesis of a site-specific ground motion. To match their spectral accelerations with S_{DS} & S_{D1}, several synthetic rock motions with a pair of distance and magnitude were first generated using the Boore's SMSIM method for the project site. A soil profile was then created using the boring log data reported by Geotechnology (2004), and the mean shear wave velocities (V_{sm}) of upper deposits (Karadeniz, 2007). Finally, site-specific response analyses were conducted with the SHAKE2000 software and the response spectra were examined to see how well they matched the design spectral accelerations, taken from the 2003 IBC. An appropriate rock motion was determined from the "best match" of these data.

For the project site located on the south side of the Old Highway "N" and east of the intersection with Highway K, the simulated rock motions predicted by the Boore SMSIM procedure were as follows: (1) M7.5 earthquake at a distance of 240 km, and (2) M7 earthquake at a distance of 100 km. These events result in spectral accelerations of approximately 0.416g at 0.14 second and approximately 0.024g at 1 second periods. The time history of the ground motions induced by both earthquakes is depicted in **Figure 15**.

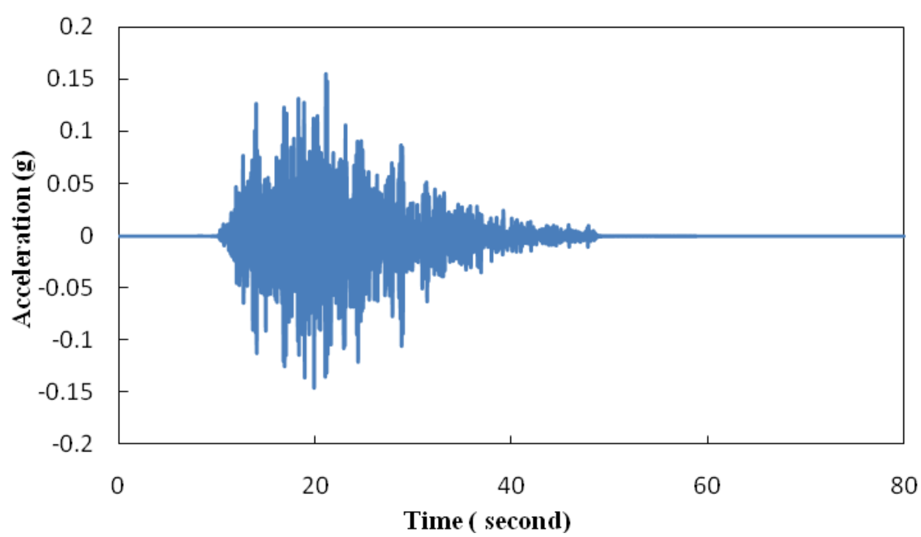

(a) M7.0 earthquake at 100 kim distance

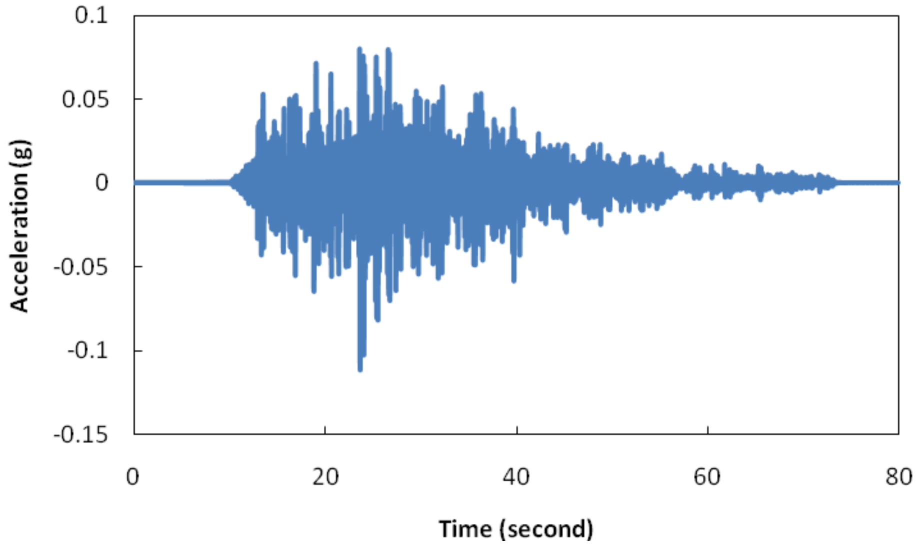

(b) M7.5 earthquake at 240 km distance

Figure 15 Synthetic ground motions at the project site

The maximum moments under one component and a combined action of two components of ground motions are presented in **Table 6** under an M7 earthquake at 100 km and in **Table 7** under an M7.5 earthquake at 240 km. In comparison with **Table 5**, **Tables 6** and **7** indicate that the maximum moment of the structure under the site specific ground motion is significantly smaller than that under the spectrum-compatible ground motion. This is attributed to different characteristics in the synthetic ground motions. The site specific ground motion depends upon the local geologic condition while the spectrum compatible ground motion was generated by following the design response spectrum that was developed based on the probabilistic seismic risk analysis.

Table 6 Maximum moment under an M7.0 earthquake at 100 km distance (kip-in)

Earthquake component	Moment	Bus #1	Bus #2	Bus #3	Bus #4	Bus #5	Bus #6
X	In-plane	0.99	0.08	1.0	0.73	0.58	0.49
	Out-of-plane	0.53	0.78	0.65	0.13	0.08	1.07
Y	In-plane	0.64	0.94	1.23	0.1	0.11	0.24
	Out-of-plane	0.63	0.29	0.66	0.82	0.23	0.55
X + 30%Y	In-plane	1.18	0.36	1.37	0.76	0.61	0.56
	Out-of-plane	0.72	0.87	0.85	0.38	0.15	1.24
30%X + Y	In-plane	0.94	0.96	1.53	0.32	0.28	0.39
	Out-of-plane	0.79	0.52	0.86	0.86	0.25	0.87
$\sqrt{X^2+Y^2}$	In-plane	1.18	0.94	1.59	0.74	0.59	0.55
	Out-of-plane	0.82	0.83	0.93	0.83	0.24	1.20

Table 7 Maximum moment under an M7.5 earthquake at 240 km distance (kip-in)

Earthquake component	Moment	Bus #1	Bus #2	Bus #3	Bus #4	Bus #5	Bus #6
X	In-plane	0.90	0.18	0.92	0.55	0.71	0.98
	Out-of-plane	0.84	0.90	1.13	0.21	0.09	1.32
Y	In-plane	0.66	0.90	1.14	0.09	0.12	0.27
	Out-of-plane	0.68	0.05	0.61	0.70	0.24	0.55
X + 30%Y	In-plane	1.10	0.45	1.26	0.58	0.75	1.06
	Out-of-plane	1.04	0.92	1.31	0.42	0.16	1.49
30%X + Y	In-plane	0.93	0.95	1.42	0.26	0.33	0.56
	Out-of-plane	0.93	0.32	0.95	0.76	0.27	0.95
$\sqrt{X^2 + Y^2}$	In-plane	1.12	0.92	1.46	0.56	0.72	1.02
	Out-of-plane	1.08	0.90	1.28	0.73	0.26	1.43

Both the out-of-plane and the in-plane moment distributions along all main buses are shown in **Figures 16** and **17** under X-component and Y-component of the M7.5 earthquake, respectively. Their distribution is similar to that under the spectrum compatible ground motion.

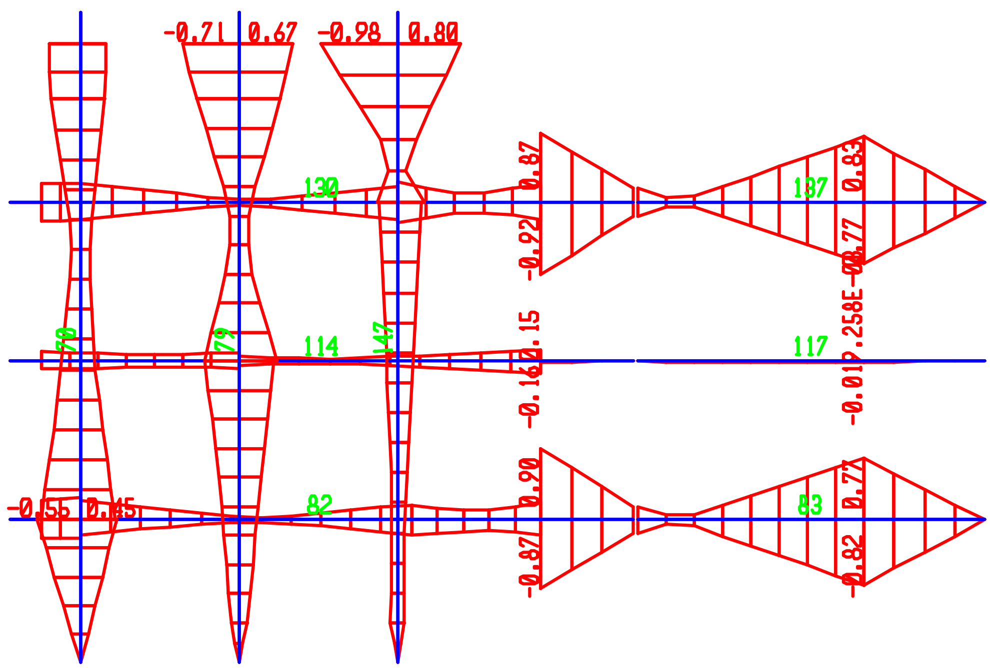

(a) Out-of-plane moment

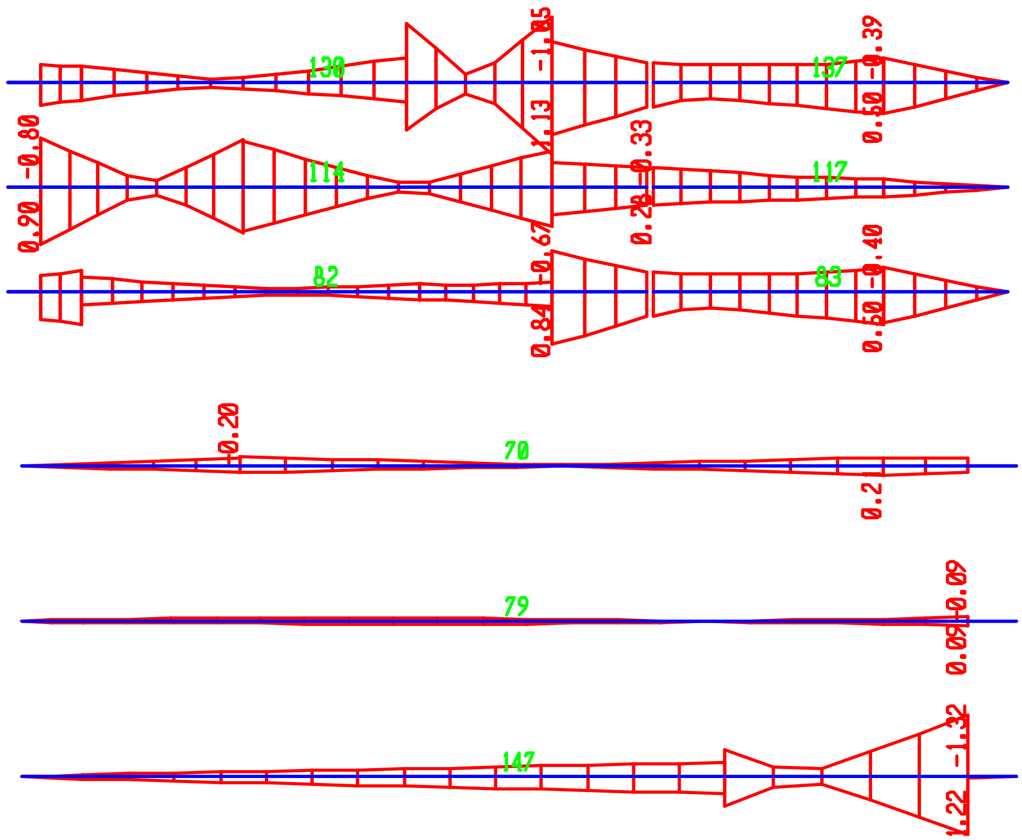

(b) In-plane moment

Figure 16 Moment envelope under X-component of the M7.5 earthquake

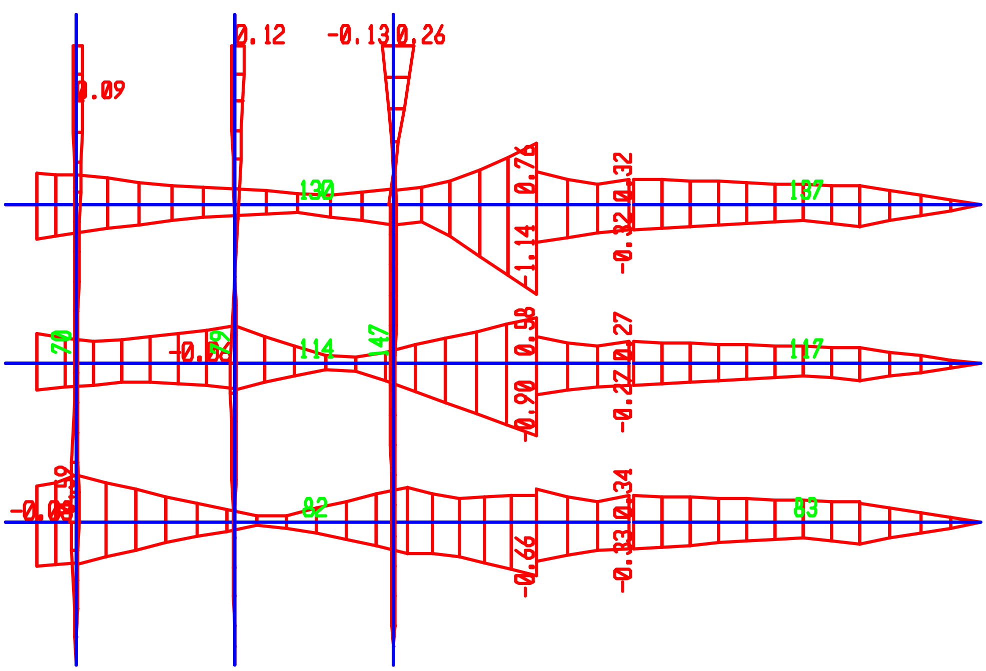

(a) Out-of-plane moment

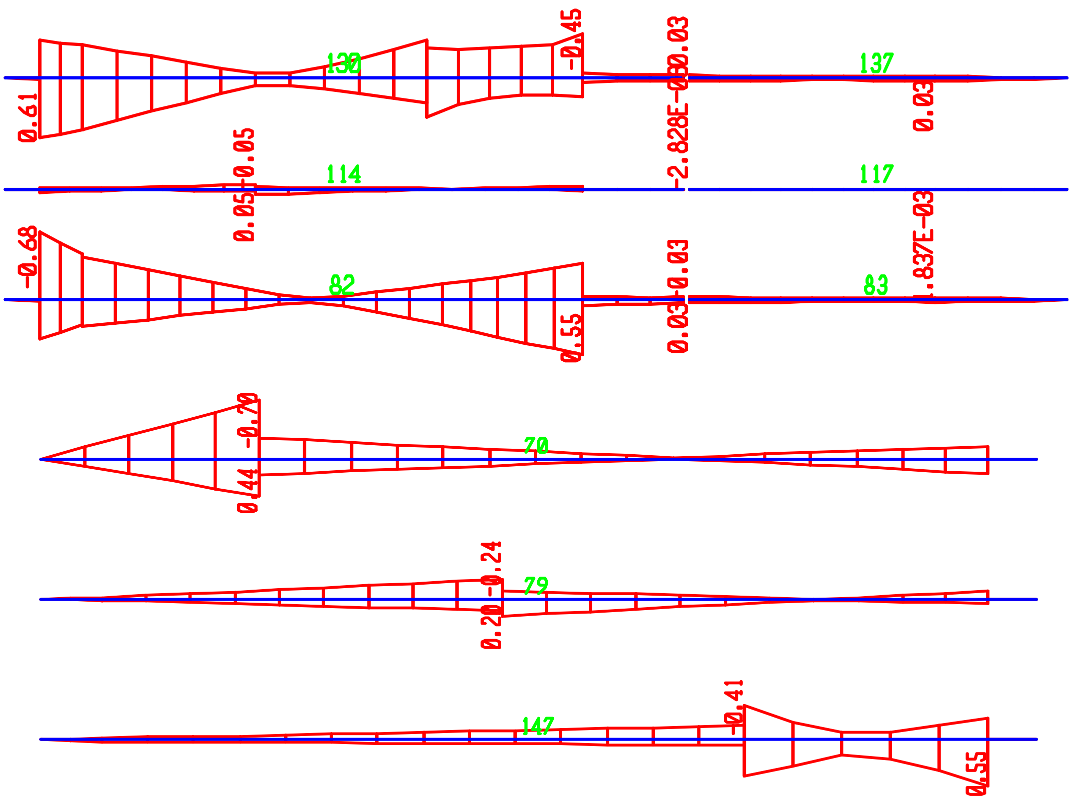

(b) In-plane moment

Figure 17 Moment envelope under Y-component of the M7.5 earthquake

6 SHAKE TABLE TEST OF SWITCHES

Electric switches are present at both levels of main buses as shown in **Figure 3**. They play a critical role in the operation of a power substation. To ensure their functionality and safety during an earthquake event, shake table tests were conducted in the Structures Laboratory at the Missouri University of Science and Technology in order to understand the behavior and potential failure mode of electric switches. Three full-size switches were provided by Turner Electric St. Louis, Missouri.

The 4’×7’ unidirectional shake table was used to excite each switch specimen. Its main dimensions are shown in **Figure 18**. Driven by one actuator that is activated by hydraulic power, the shake table can operate in the frequency range from 0.01 Hz to 10 Hz with a maximum payload of 20 tons. The maximum stroke of the table is +/-1.0”. The MTS407 controller has a function generator such as sine and cosine waves. The table can also take external signals to simulate any earthquake ground motion.

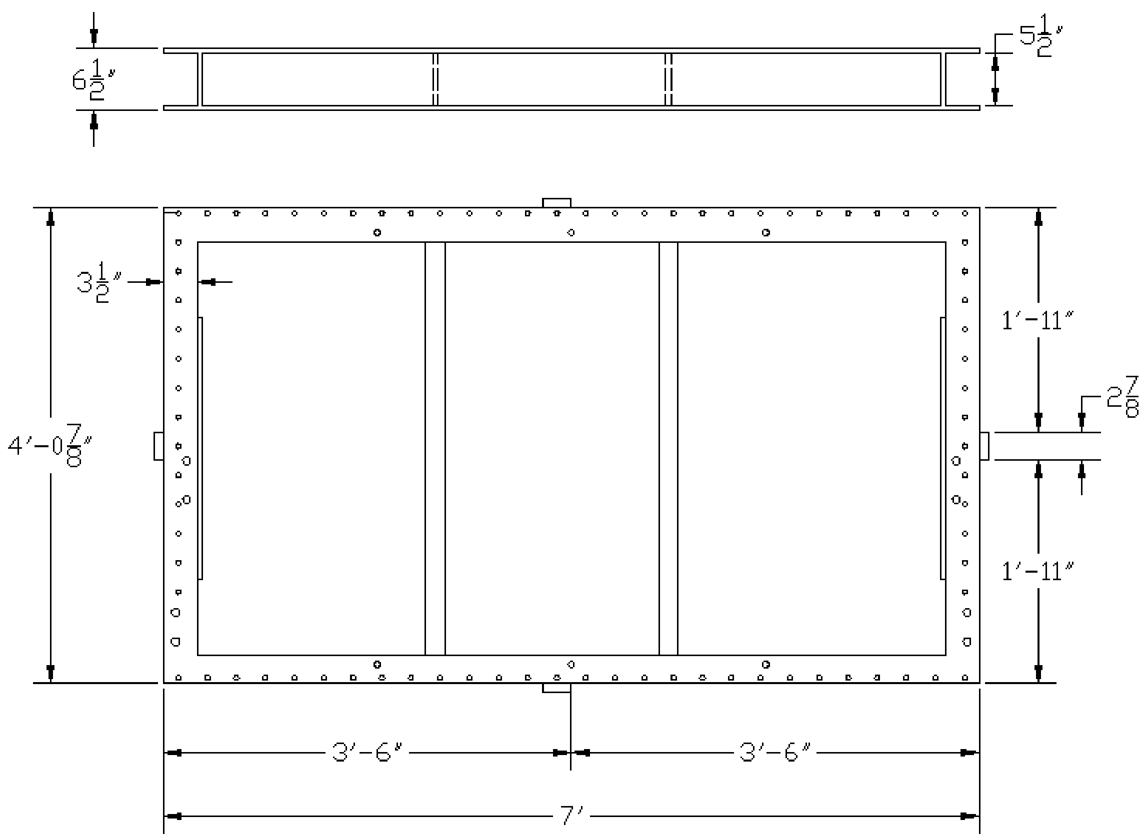

Figure 18 Dimensions of the shake table

6.1 Test setup and instrumentation

Each test specimen provided by Turner Electric has three porcelain pillars that are supported on a hollow square cold-formed steel tube. To extend the support length for the switch specimen, an "I" beam was designed and bolted onto the shake table as illustrated in **Figure 19**. In this study, the switch was tested for the dynamic behavior in the plane formed by the three pillars. To maintain the lateral stability during shake table tests, a simple wood truss was built and used as top transverse supports to the switch, as shown in **Figure 20**. The top horizontal wood member along the excitation direction is placed near the test specimen with a small gap in between.

Each switch has a mechanical mechanism that is used to open and close the electric switcher or the aluminum bus. As shown in **Figure 19**, the switcher was rigidly connected to the center pillar. One end of the mechanism was clamped to the porcelain pillar and the other end was hinged to a metal shaft that passes through a hollow porcelain pillar and is rigidly connected to the base beam made of a hollow square tube. The base beam provides supports for the other two pillars as well.

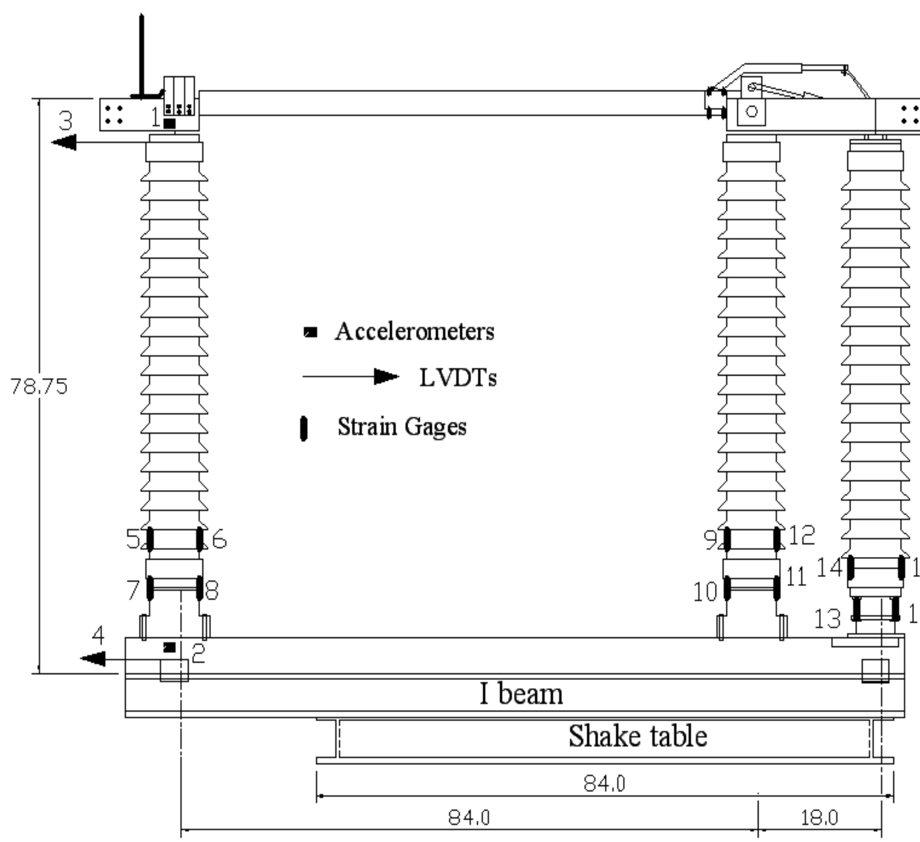

(a) Switch No.1 (all dimension in inches)

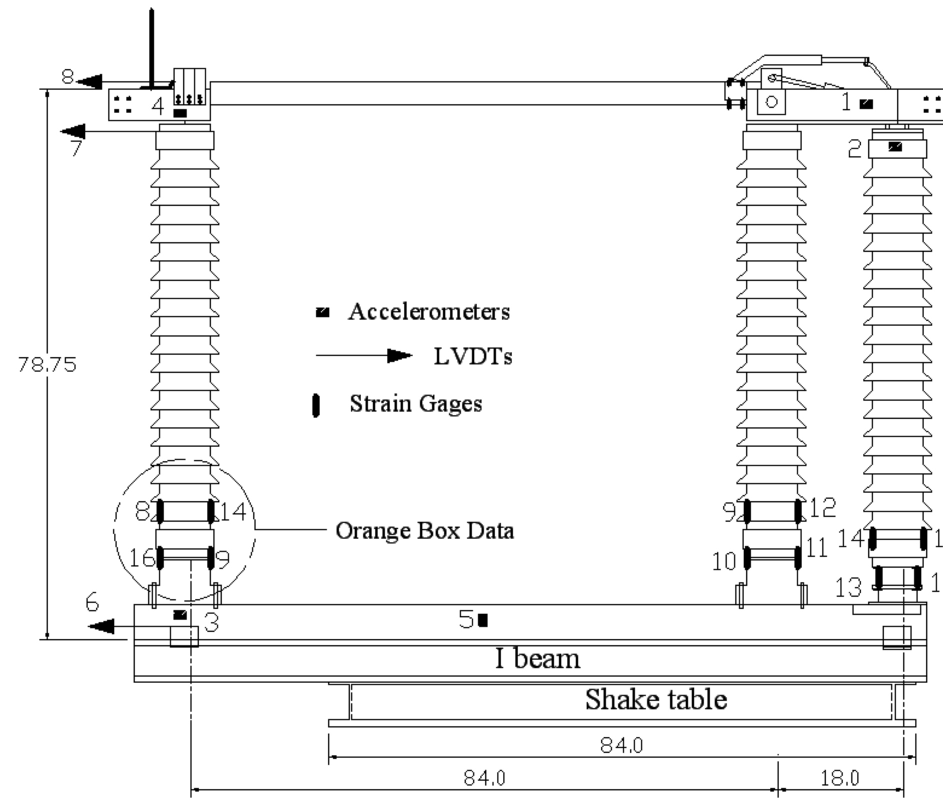

(b) Switches No. 2 (all dimensions in inches)

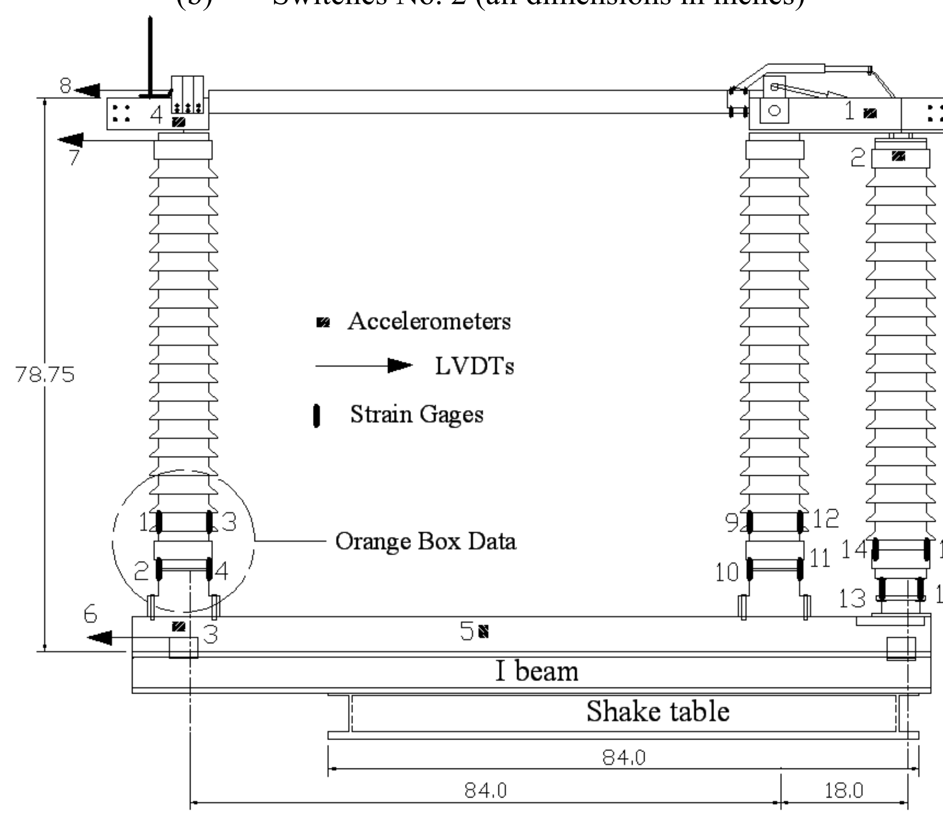

(c) Switches No. 3 (all dimensions in inches)

Figure 19 Test setup and instrumentation of Turner TMX B104 vertical break switches

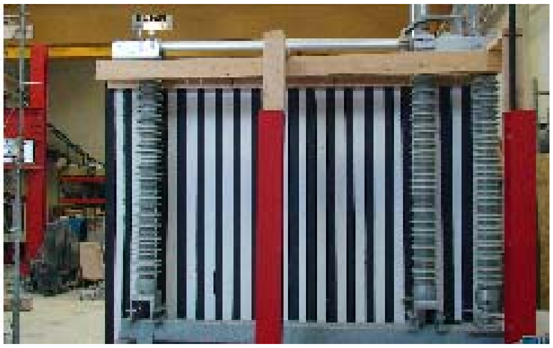

Figure 20 Wood truss system

Figure 21 Two data acquisition systems

Each switch was instrumented with accelerometers, LVDTs, and strain gauges as illustrated in **Figures 19**(a-c) for the 1st, 2nd, and 3rd switches. At the completion of the 1st switch test, new observations were made and the instrumentation was modified for the 2nd and 3rd switches in addition to the availability of different data acquisition systems. As shown in **Figure 21**, the 8-channel Synergy Box and the Orange Box were used for the 1st switch while the upgraded 16-channel Synergy Box and the Orange Box were used to acquire data from the shake table tests of the 2nd and 3rd switches. The Synergy Box was used to take accelerations and displacements as well as most of strain gauges. The Orange Box was used to read from several strain readings. Video images were also taken during some of the shake table tests. To enhance the video quality, a screen with marked strips was provided in the back of the test specimen.

As illustrated in **Figure 19**(a), Switch #1 was instrumented with two accelerators, two linear variable differential transformer (LVDTs), and twelve strain gauges. The two accelerometers were installed on the bottom and top of the left porcelain pillar for horizontal acceleration measurements. Two linear variable differential transformers (LVDTs) were installed at the bottom and top of the left pillar to measure their dynamic displacements. Twelve strain gauges were installed at various locations on pillars and their end supports as shown in **Figure 19**(a).

As illustrated in **Figure 19**(b, c), Switch #2 and #3 was each instrumented with three accelerators, three LVDTs, and twelve strain gauges. The three accelerometers were installed on the bottom and top of the left porcelain pillar for horizontal acceleration measurements as well as in the mid span of the bottom hollow square tube for vertical acceleration measurement. The three LVDTs were installed at the bottom and top of the left pillar as well as at the switch to measure their dynamic displacements. Twelve strain gauges were installed at various locations as shown in **Figure 19**(b, c).

6.2 Excitation and test procedure

Each specimen was excited with a sinusoidal motion in a frequency range 4 to 10 Hz in 0.2 Hz interval. When the electric switch was closed, all LVDTs were set to zero prior to testing. For each test run, the excitation frequency was set and controlled by the MTS407 Controller. However, the stroke of the shake table was manually set and gradually increased to a predetermined value, e.g., 0.1”, to minimize a potential jerk that the shake table system could generate otherwise, potentially damaging the specimen unintentionally. In its steady state, the maximum displacement can be applied for 15 sec. or longer to acquire the steady-state data. As a result, each run at any excitation frequency will last over 30 sec., which is governed by the lower bound of excitation frequency.

The specific objectives of the shake table tests are to evaluate the dynamic characteristics (natural frequency and damping ratio) and identify the failure modes of typical electric switches. To this end, the following test procedure was adopted:

Step 1: Conduct a series of harmonic tests with constant amplitude and increasing excitation frequency.

Step 2: Repeated Step 1 with an increase in the amplitude of the excitation.

Step 3: Excite the structure at its fundamental frequency with an increment of increasing amplitude.

6.3 Frequency transfer function estimates

Fast Fourier Transformation (FFT) is an effective tool for transforming a measured signal from time domain to frequency domain. As an example, a two-frequency-component signal, $x(t) = \sin(2\pi \times 40t) + \sin(2\pi \times 15t)$ as illustrated in **Figure 22**(a), results in the FFT as shown in **Figure 22**(b) with two distinct frequency components: 15 Hz and 40 Hz.

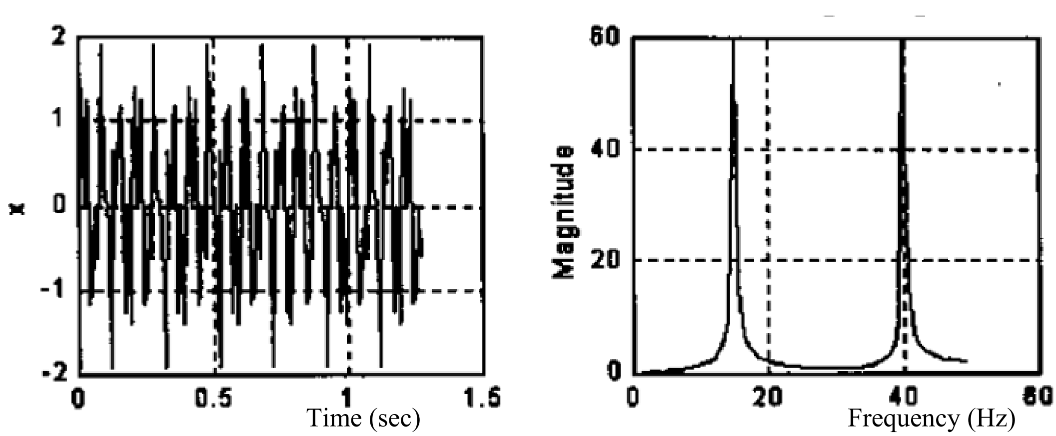

(a) Time history (b) FFT

Figure 22 Time history and Fourier transform

Power Spectrum Density (PSD) will be used to identify the natural frequency of electric switches when subjected to harmonic excitations. It can be readily derived from the Fourier Transform as briefly described below. For each switch, the structural response can be related to the input excitation by their frequency response function (FRF), H(ω), as illustrated in **Figure** :

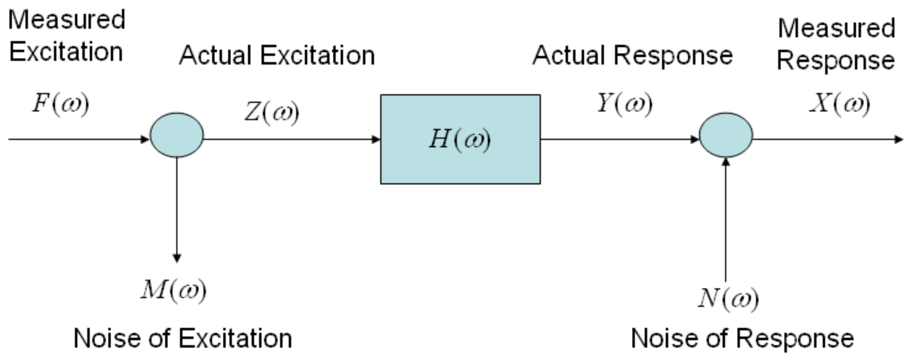

Figure 23 Relationship between excitation and response

Mathematically, the relation between the actual response Y(ω) and the actual excitation Z(ω) in frequency domain can be described as:

$$X - N = H(F - M) \tag{6}$$

in which Z(ω) = F(ω) - M(ω) is the Fourier transform of the actual excitation and Y(ω) = X(ω) - N(ω) is the Fourier transform of the actual response; F(ω) and X(ω) represent the measured excitation and structural response, respectively; M(ω) and N(ω) represent measurement noises to the excitation and structural response, respectively.

The excitation measurement noise only modifies the measured excitation and does not affect the actual excitation to the shake table. The response measurement noise will directly affect the ability of identifying structural characteristics. In the case of no excitation noise, Eq. (6) becomes:

$$N = X - HF \tag{7}$$

For *m* identical tests, the total amount of noises can be measured by:

$$J = \sum_{i=1}^{m} |N_i|^2 = \sum_{i=1}^{m} (X_i - HF_i)(X_i - HF_i)^* \tag{8}$$

The noise can be minimized by letting $\partial J / \partial H^* = 0$, resulting in the following estimated FRF:

$$\hat{H}(\omega) = \sum_{i=1}^{m} X_i F_i^* / \sum_{i=1}^{m} F_i F_i^* = \hat{G}_{fx}(\omega) / \hat{G}_{ff}(\omega) \tag{9}$$

Here, $\hat{G}_{fx}(\omega)$ and $\hat{G}_{ff}(\omega)$ are the cross- and auto-spectrum density functions, respectively.

6.4 Structural identification with force vibration tests

The natural frequency and damping ratio of each switch structure can be identified with the half-power method and the peak method using the estimated FRF. Two example FRFs are discussed below. Other FRFs at different excitation frequencies are included in Appendix.

Under a theoretic harmonic excitation with an excitation frequency of 7.6Hz and a displacement stroke of 0.05 in, the structure of Switch No.2 is subjected to a table acceleration shown in **Figure 24**(a) and experiences the displacement at the top of the isolated porcelain pillar in **Figure 24**(b).

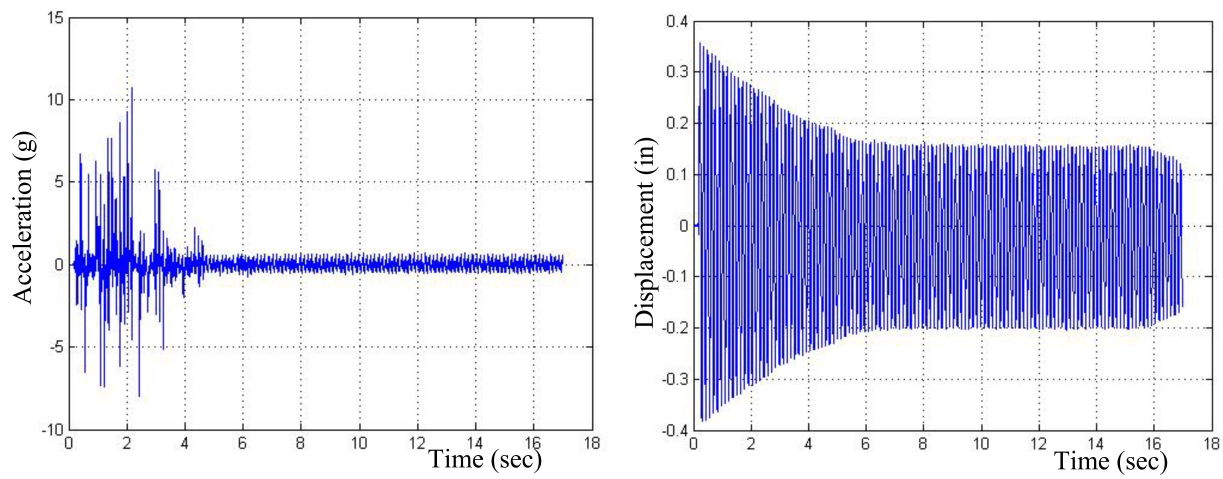

(a) Table acceleration (b) Top displacement

Figure 24 Excitation and response of Switch No.2

The FRF of the top displacement of the left pillar with respect to the table acceleration as shown in **Figure 24** is presented in **Figure 25**. It can be observed from **Figure 25** that the frequency corresponding to the peak FRF value is approximately 7.33 Hz. The damping ratio is approximately 3%.

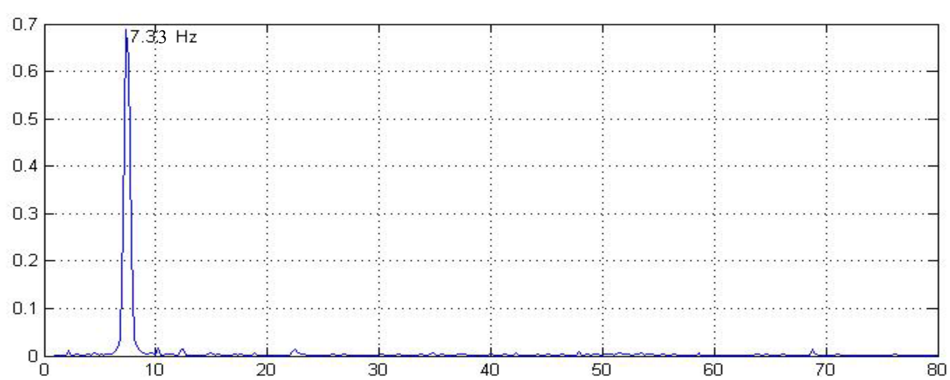

(a) Absolute value (modulus)

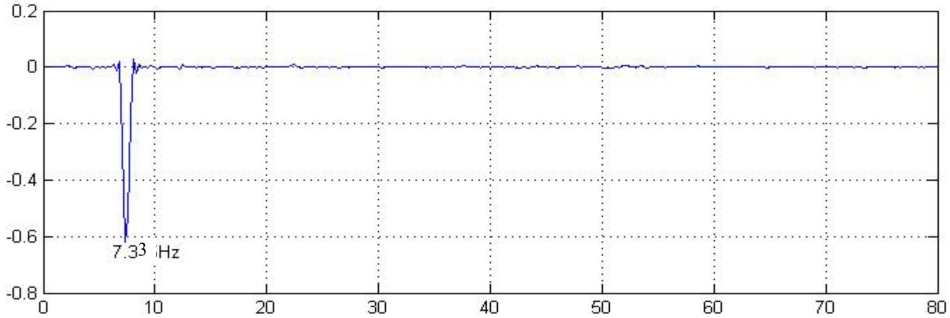

(b) Real part

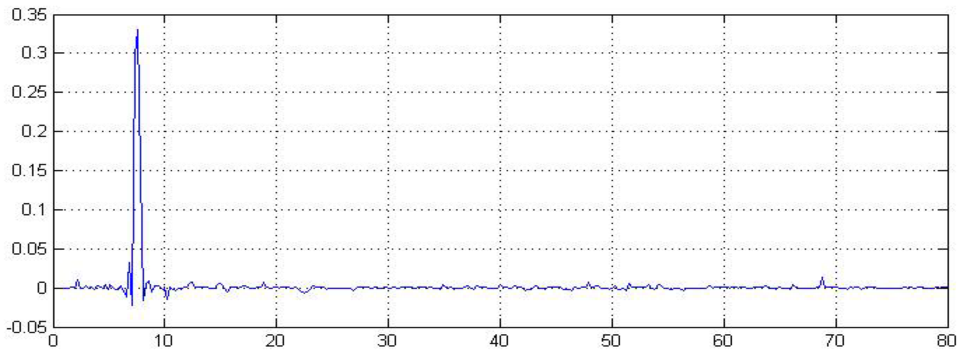

(c) Imaginary part

Figure 25 FRF with an excitation frequency of 7.6 Hz: Switch No. 2

Similarly, the FRF of the switch No. 2 under a theoretic harmonic excitation of frequency 7.8 Hz with a stroke of 0.05 in is presented in **Figure 26**. In this example, the FRF is presented in the logarithmic scale, showing three distinct peaks corresponding to the first three vibration modes. Like the previous example, the fundamental frequency identified is smaller than the excitation frequency. However, the identified fundamental frequencies from the two examples are within 4% error.

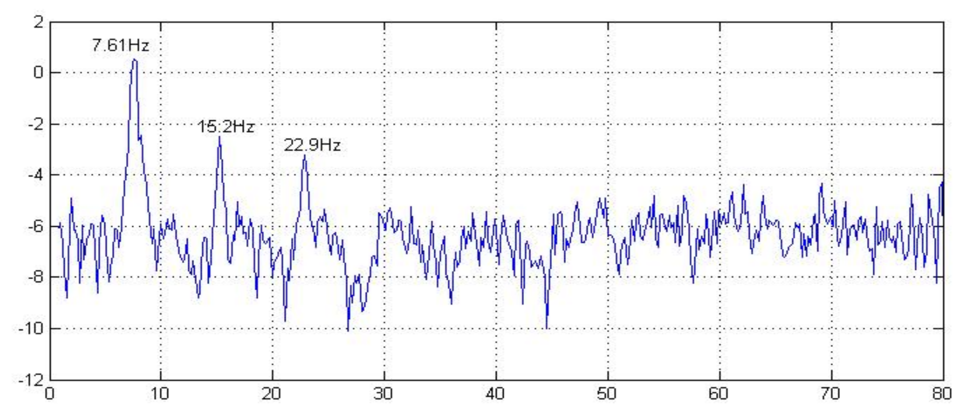

(a) Absolute value

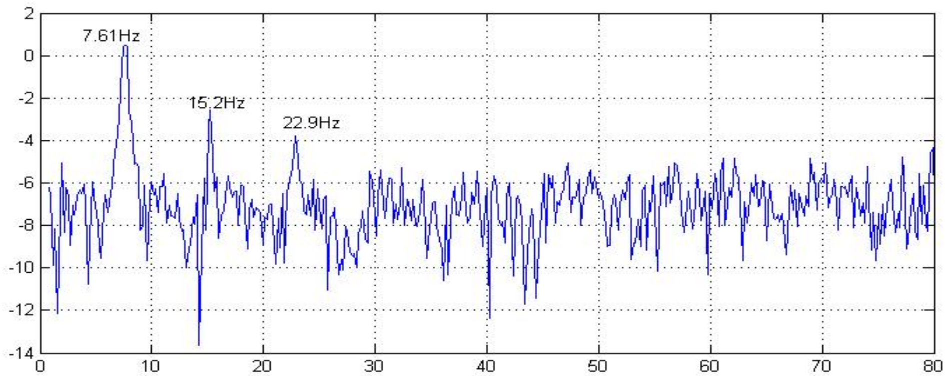

(b) Real part

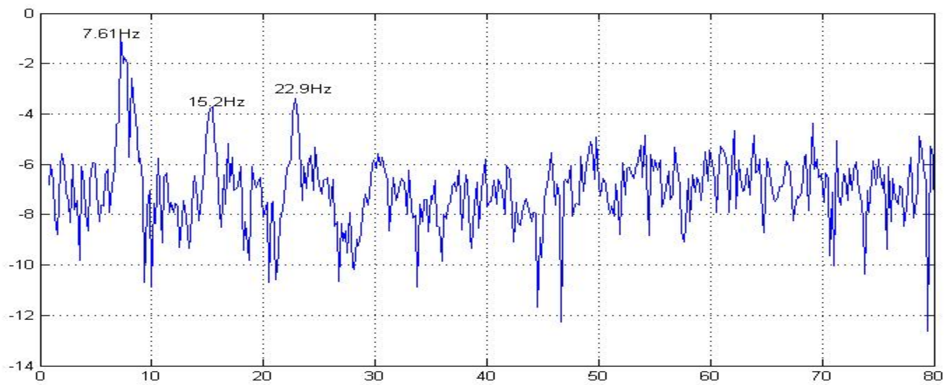

(c) Imaginary part

Figure 26 FRF at 7.8 Hz excitation frequency: Switch No.2

The identified natural frequencies from various forced vibration tests with different excitation frequencies are summarized in **Table 8**. As clearly shown in Table 8, the identified fundamental frequency varies within 1.8% with an average value of 7.41 Hz. Based on the peak responses observed during the shake table tests, the fundamental frequency seems close to 7.61 Hz with corresponding second and third frequencies of 15.2 Hz and 22.9 Hz, respectively. The actual fundamental frequency of the test switch, No.2, most likely ranges from 7.30 to 7.61 Hz. Similarly, the fundamental frequency of Switch No. 3 was identified to be 7.5 Hz.

Table 8 Natural frequencies of Switch No. 2

Excitation frequency (Hz)	1st natural frequency (Hz)	2nd natural frequency (Hz)	3rd natural frequency (Hz)
7.2	7.32	-	-
7.4	7.30	-	-
7.6	7.33	-	-
7.8	7.61	15.2	22.9
8.0	7.50	-	-
Average	7.41	-	-

6.5 Structural identification with free vibration tests

Free vibration tests were conducted on Switch No. 2. A representative free vibration response is presented in **Figure** . The damping ratio can then be estimated from the free vibration by $\varsigma = \ln(u_i / u_{i+j}) / 2\pi j$, in which u_i and u_{i+j} denote the i^{th} and $i+j^{th}$ peak displacements, respectively. The identified damping ratio is 2.8% for Switch No.2. The fundamental natural frequency identified from the free vibration is approximately 8 Hz. This value is nearly 8% higher than that identified from the force vibration.

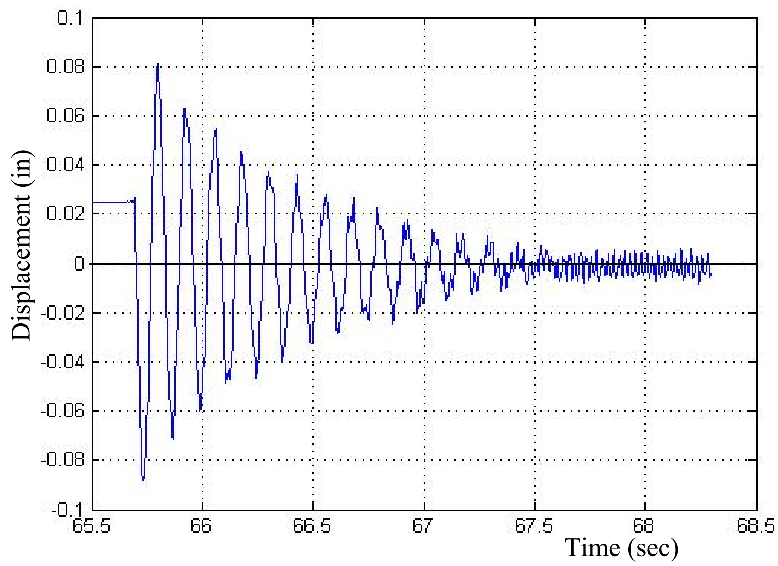

Figure 27 Free vibration of Switch No.2

6.6 Modal analysis of the specimen

A FEM of the switch specimen was established as shwon in **Figure** . The Young's moduli of the porcelain and steel materials are taken to be 28,993 ksi and 29,000 ksi. The specific weights per volume are assumed to be 8.67×10^{-5} kip/in^3 and 2.84×10^{-4} kip/in^3. To simulate the low frequency vibration, each member of the switch structure was modeled by a frame element in SAP2000. As a result, the model has a total of nine elements and six joints. At the switcher, the clamped mechanism was modeled by a link element that allows for free movement in horizontal direction but restrained in vertical motion. A spring element was used to simulated the hinged metal shaft. Based on the modal analysis, the first three natural frequencies are 7.68 Hz, 14.1 Hz, and 23.8 Hz, respectively. Their corresponding mode shapes are shown in **Figure 29**. The difference of this identified frequency from the theoretical excitation frequency is likely due to the mechanical "noise" or the modification of the theoretical excitation by the shake table and the test apparatus (the I-beam).

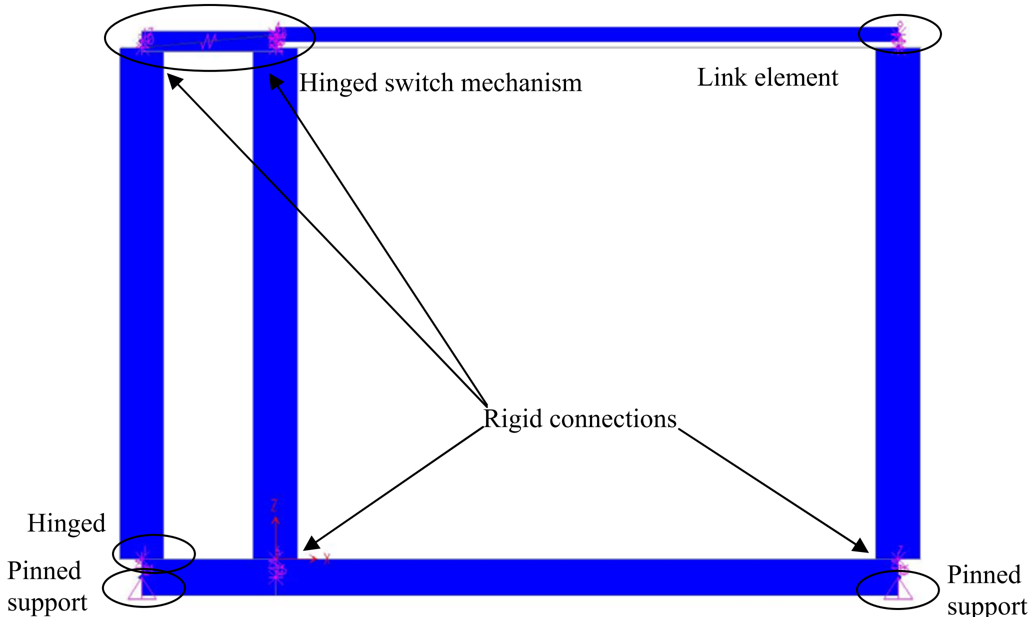

Figure 28 FEM of the switch specimen

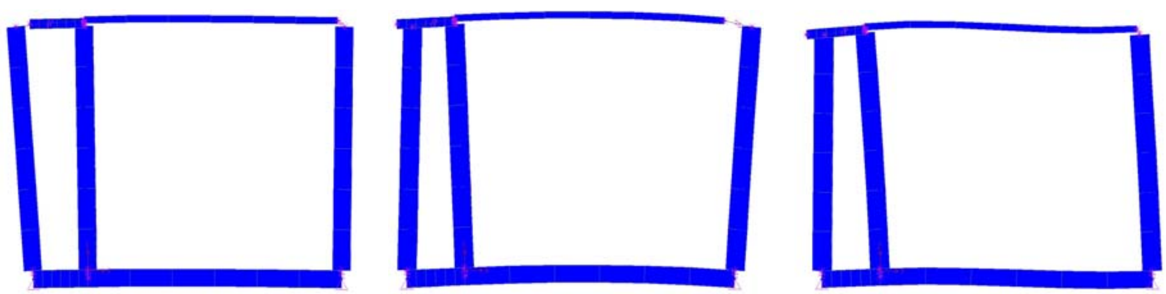

(a) 1st Mode (b) 2nd Mode (c) 3rd Mode

Figure 29 Mode shapes of the specimen

6.7 Break tests

The fundamental frequency, 7.61 Hz, identified from the force vibration of Switch No.2 was considered as excitation frequency for break tests. To test the failure behavior, the displacement amplitude of the excitation was increased manually to 0.2 in. The table acceleration (actual excitation to the specimen) and the displacement response are presented in **Error! Reference source not found.** (a, b), respectively. As shown in **Figure 30** (b), the maximum displacement from LVDT 8 was 1.76 in prior to breaking of the switch system.

The break test of Switch No.3 was first conducted at an excitation frequency of 7.2 Hz based on the vibration observation during the previous shake table tests. However, it was observed that the vibration attenuated significantly and the excitation frequency was lowered to 7.0 Hz. The switch response continued to decrease at 7.0 Hz. Finally, the switch system was excited at 6.7 Hz with a stroke of up to 0.3 in. The table acceleration of the excitation is presented in **Figure 31** (a). **Figure 31** (b) shows the displacement measured from LVDT 8, and the switch system failed at the maximum displacement of 1.5 in at 22 sec.

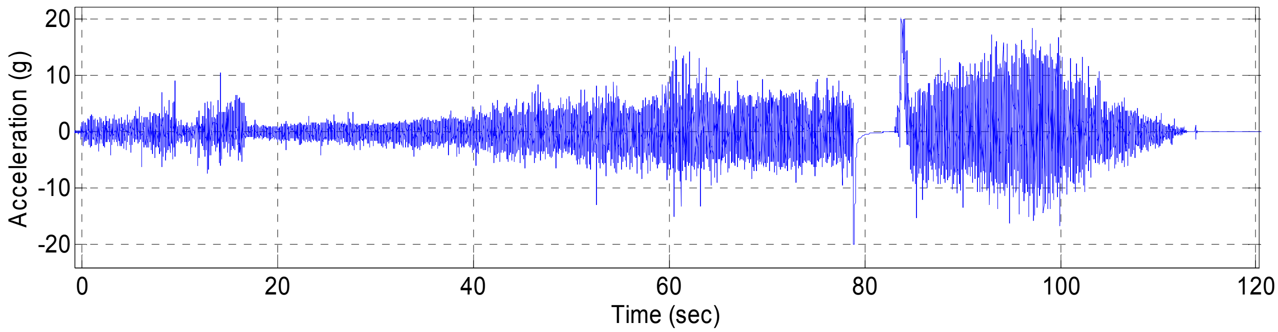

(a) Excitation: table acceleration

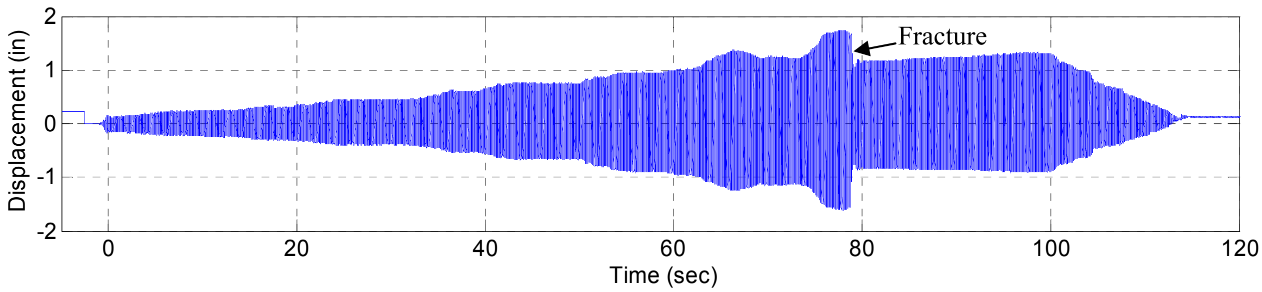

(b) Response: electric switch displacement at the top of the pillar

Figure 30 Break test results of Switch No.2

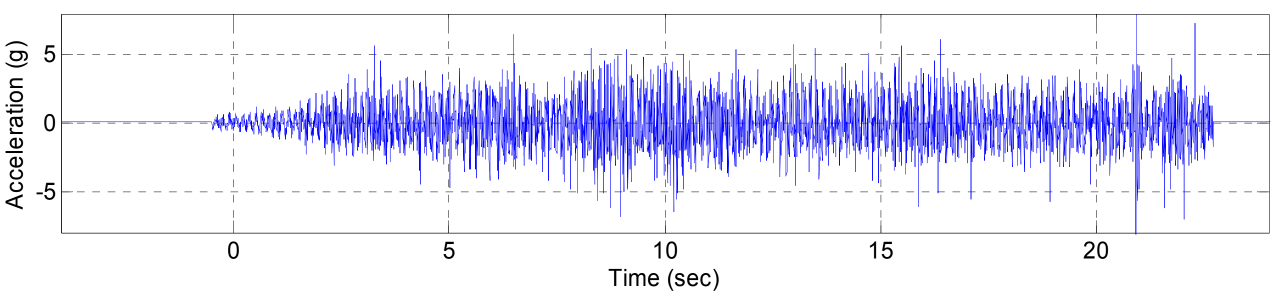

(a) Excitation: table acceleration

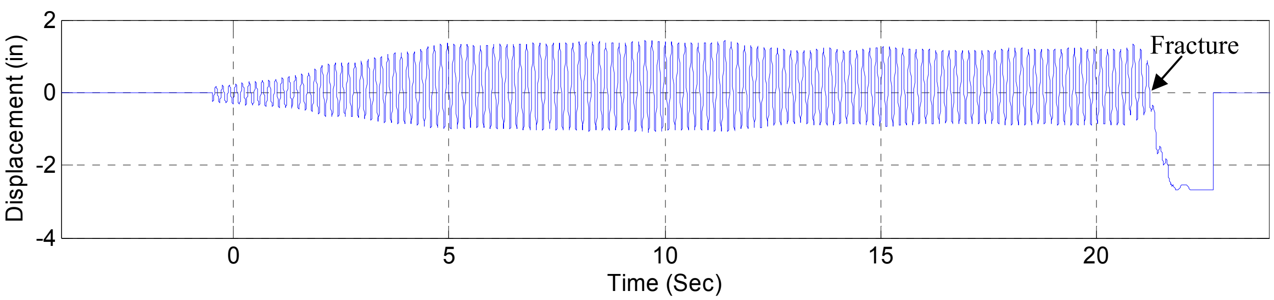

(b) Response: electric switch displacement at the top of the pillar

Figure 31 Break test results of Switch No.3

All three test specimens consistently fractured at the bottom end of the metal shift as part of the open-and-close mechanism of the electric switches. These were likely due to the combined effects of fatigue and initial defect prior to testing. A typical failure mode is illustrated in **Figure 32**.

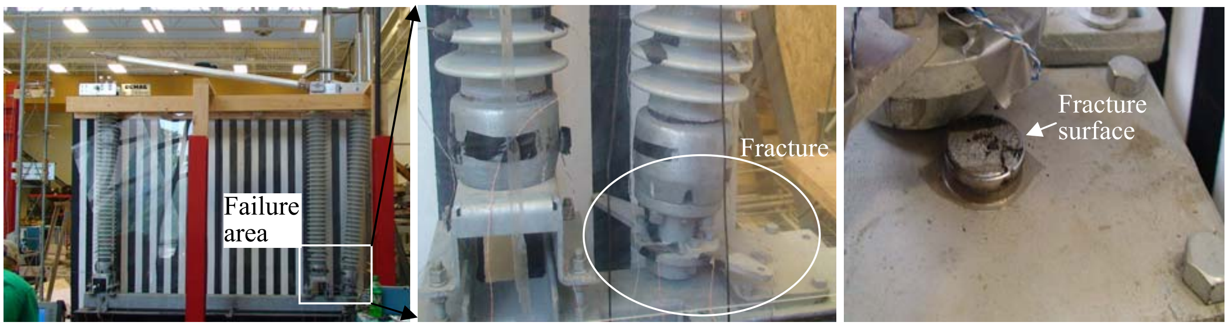

(a) Switch system (b) Area of fracture (c) Fracture surface

Figure 32 Failure mode of Switch No.3

6.8 Time-varying frequency identification

During the shake table tests, the aluminum bus (electric switcher) was found to occasionally slide against its supporting porcelain pillar, particularly at resonance. When the slip-stick motion at the switcher occurs frequently, the natural frequency of the switch system will change with time. For example, the FEM gives a natural frequency of 8 Hz for the entire switch system in close position. Once in open position, the switch system becomes two separate parts: a two-pillar part and a single pillar. Their natural frequencies are 7.7 Hz and 11.0 Hz, respectively. As far as the horizontal vibration is concerned, the open position of the switcher is equivalent to the sliding motion between the bus and its supporting pillar. In this section, an attempt was made to identify the change of natural frequency of Switch No. 3. For this purpose, the least-square estimation method was applied as an efficient approach in time domain. In order to identify the frequency variation over time at resonance, a slide-window least-square estimation with an enhanced approach to update the slide window was developed.

Based on the conventional least square estimation, the identified fundamental frequency is approximately 7.5Hz and the average damping ratio is 4.8%, both consistent with those observed during testing. However, as shown in **Figure 33**, the natural frequency was suddenly reduced near resonance.

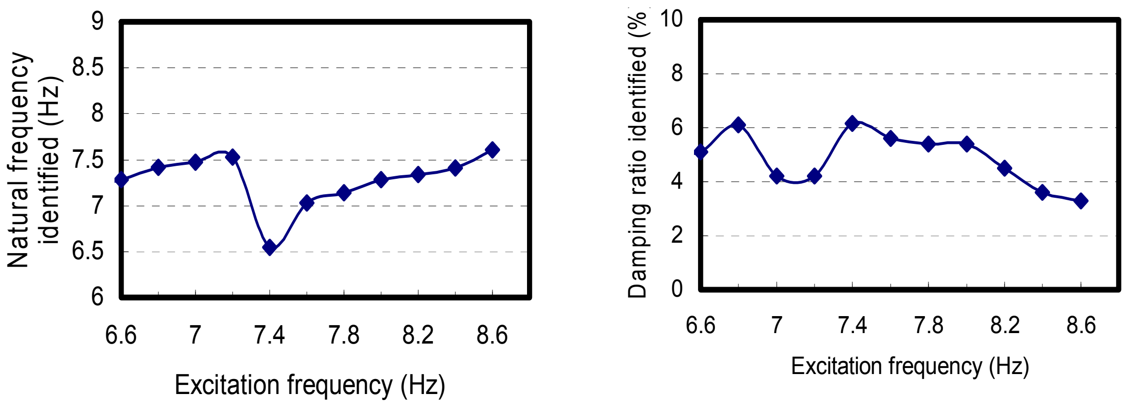

(a) Frequency variation (b) Damping variation

Figure 33 Fundamental frequency and damping ratio identified of Switch No.3

Based on a slide-window least-square estimation with an enhanced approach to update the slide-window, frequency variation over time at resonance was identified. **Figure 34** presents the relative displacement between the electric switcher and its supporting pillar (LVDTs 7 versus 8) and the identified fundamental frequency. It can be observed from **Figure 34** that when the relative displacement between the aluminum bus (electric switcher) and the top of the porcelain pillar remained constant over time, the natural frequency was also constant. The natural frequency was 7.5 Hz as shown in **Figures 34** (a). The small relative displacement at the switcher is an indication of no slippage during the shake table tests. The non-zero displacement is most likely a result of noise effects.

Figure 34 (b) demonstrates that when the relative displacement between the bus and the top of the pillar varied over time, the natural frequency identified changed. From -2.0 to 0.8 sec., the relative displacement between the bus and the top of the pillar was small, and the natural frequency identified was 7.5 Hz, which is consistent with that identified from different forced vibration tests as illustrated in **Figure 34** (a, d). From 0.8 to 3.4 sec., as the relative displacement varied from -0.01 in to 0.12 in, the natural frequency decreased from 7.5 Hz to 6.3 Hz. From 3.4 to 5.4 sec., the relative displacement decreased to 0.09in, and the natural frequency increased to 6.5 Hz. From 5.4 to 14.0 sec., the relative displacement remained constant, and the natural frequency remained at 6.5Hz, indicating that the switch system did not return to its initial condition when the switch was in close position. At the end of excitation, the relative displacement decreased to 0.04in, and the natural frequency increased to 7.0Hz.

Figure 34 (c) shows that from -0.5 to1.0 sec., the relative displacement between the bus and the top of the pillar was a small constant value, the natural frequency was identified to be 7.25 Hz. The difference of this identified frequency from 7.5 Hz was due likely to the residual relative displacement from the previous tests. From 1.0 to1.5 sec., as the relative displacement varied from -0.04 in to 0.05 in, the natural frequency decreased from 7.25 Hz to 7.0 Hz. From 1.5 to14.0 sec., the relative displacement remained 0.05 in, and the natural frequency was 7.0 Hz. At the end of excitation, the relative displacement decreased to 0.025 in and the natural frequency increased to 7.6 Hz.

As shown in **Figure 34** (d), the relative displacement between -1.2 and 0.0 sec. was constant and close to zero, and the natural frequency was 7.4 Hz. From 0.0 to14.0 sec., the relative displacement varied from 0 to 0.01 in, and the natural frequency decreased to 7.3 Hz. At the end of excitation (from 14 to16sec.), the relative displacement decreased to zero and the natural frequency increased again to 7.5 Hz.

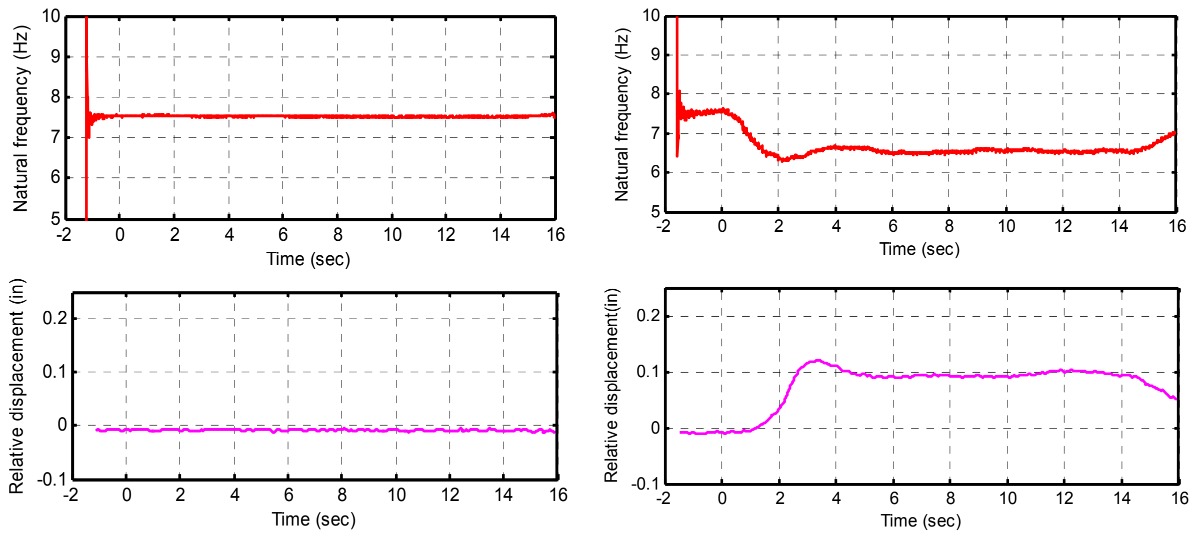

(a) Excitation frequency = 7.0 Hz (b) Excitation frequency = 7.2 Hz

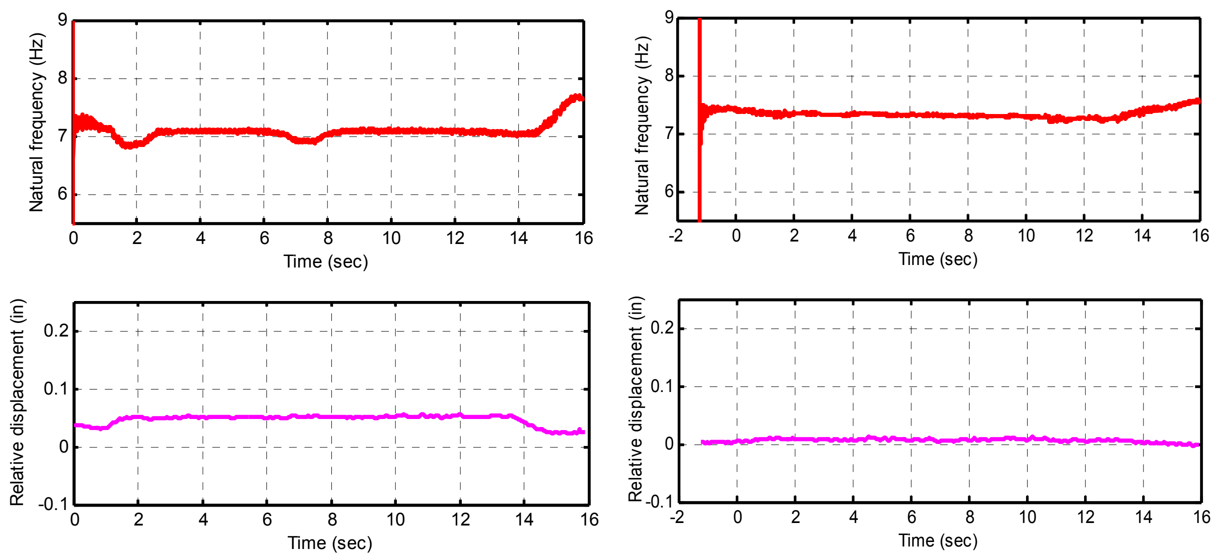

(c) Excitation frequency = 7.6 Hz (d) Excitation frequency = 8.2 Hz

Figure 34 Relative displacement and fundamental frequency identified over time

7 REMARKS

1. The three-dimensional responses of the electric substation structure are evident. Most of the vibration modes are coupled together. The dynamic characteristics (frequency and mode shapes) of the structure indicate that the cable-stayed structure is flexible in both horizontal directions.
2. The 20 significant modes of vibration up to 7.08 Hz include more than 90% mass participations in both horizontal directions. The fundamental period of the switch system is 0.826 sec.
3. Based on the response spectrum analysis, the maximum moment of 12.4 kip-in occurs in Bus 2 of the switch system. The maximum relative displacement at the slip joint of all buses is up to 2.24 inches. In general, the out-of-plane motion is significantly stronger than the in-plane response of the bus-supported frame.
4. Based on the time history analysis with synthetic ground motions, the maximum moment is approximately 12.44 kip-in, comparable to that obtained from the response spectrum analysis. The maximum relative displacement at the slip joints is 1.86 inches, 17% lower than the result from the response spectrum analysis. This conclusion mainly results from the fact that the response spectrum analysis loses the phase information among various responses, thus amplifying the relative motion.
5. From the shake table tests, the first three natural frequencies of the switch system are approximately 7.41 Hz, 15.2 Hz and 22.9 Hz, respectively. They are much higher than their corresponding natural frequencies of the overall substation structure. The damping ratio is approximately 2.8%.
6. The break tests indicated that the three tested specimens consistently fractured at the bottom of a metal shaft as part of the open-and-close mechanism. The maximum displacement at the top of pillars or the location of the electric switcher is 1.76 in.
7. It was observed that the natural frequency of the switch system changes with time as the switch structure experiences significant vibration. This is due to the slip and stick alternating process of the electric switcher.

ACKNOWLEDGEMENT

Financial support to complete this study was in part provided by Ameren and by the Center for Transportation Infrastructure and Safety.

REFERENCES

1. Kazuo Konagai, Nelson E. Pulido and Teturou Yamamoto et al. "The journal 13, 2001 off the coast of EL Salvador Earthquake," Earthquake Engineering Committee, Japan Society of Civil Engineers, August, 2001.
2. Armen Der Kiureghian, Jerome L. Sackman and Kee-Jeung Hong. "Interaction in interconnected electrical substation equipment subjected to earthquake ground motions," Report No. PEER 1999/01, Submitted to Pacific Gas & Electric Co., San Francisco, California. February, 1999.
3. Armen Der Kiureghian, Kee-Jeung Hong and Jerome L. Sackman. "Further studies on seismic interaction in interconnected electrical substation equipment," Report No. PEER 2000/01, Pacific Earthquake Engineering Research Center, College of Engineering, University of California, Berkeley, November, 1999.
4. Junho Song, Armen Der Kiureghian and Jerome L. Sackman. "Seismic response and reliability of electrical substation equipment and system," Report No. PEER 2005/16, Pacific Earthquake Engineering Research Center, College of Engineering, University of California, Berkeley, April, 2006.
5. Geotechnology Inc. "Subsurface exploration highway 'N' substation in O'Fallon, Missouri," Report-IN/739001SE, 2004.
6. International Code Council. *International Building Code (IBC)*, Section 1615, p.322-307, 2003.
7. D. Karadeniz. "Pilot program to assess seismic hazards of the Granite City, Monks Mound, and Columbia Bottom Quadrangles, St. Louis Metropolitan Area, Missouri and Illinois," Ph.D. Dissertation Submitted to the Graduate Faculty in the Department of Geological Sciences and Engineering at Missouri University of Science and Technology, unpublished, 2007.
8. Tom Irvine. *An Introduction to Frequency Response Functions*. August 11, 2008
9. Anil K. Chopra. *Dynamics of Structures*, Prentice Hall, 2nd Edition, 2001.

10. Randall Allemang. “Chapter 5: frequency response function measurements,” +UC-SDRL-RJA CN-20-263-663/664.

11. M. Bodson. “An information-dependent data forgetting adaptive algorithm,” Proceedings of the 1995 American Control Conference, June 1995.

12. Ravindra V. Jategaonkar. *Flight Vehicle System Identification - a Time Domain Methodology*, American Institute of Aeronautics and Astronautics, Inc., VA, 2006.

13. Jann N. Yang, and S. Lin. “Identification of parametric variations of structures based on least squares estimation and adaptive tracking technique,” Journal of Engineering Mechanics, Vol. 131, No. 3, 2005, pp. 290–298.

APPENDIX: FREQUENCY RESPONSE FUNCTION FROM VARIOUS TESTS

A1 Excitation frequency = 6.8 Hz

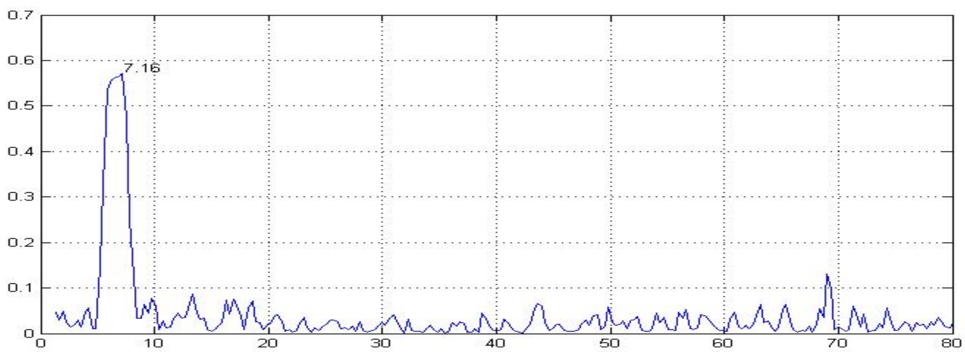

(a) Absolute value of FRF

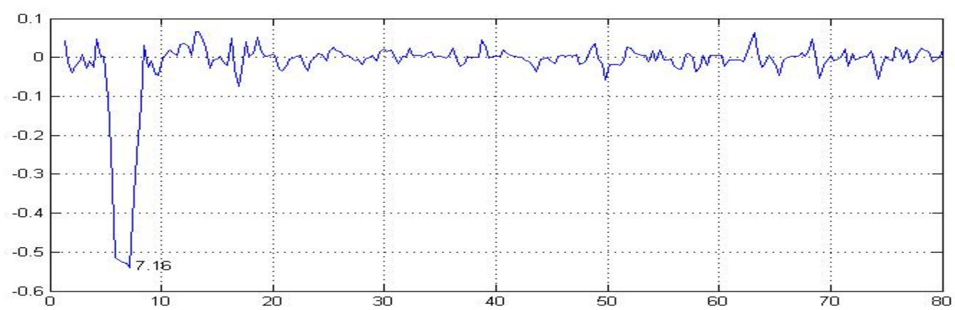

(b) Real part of FRF

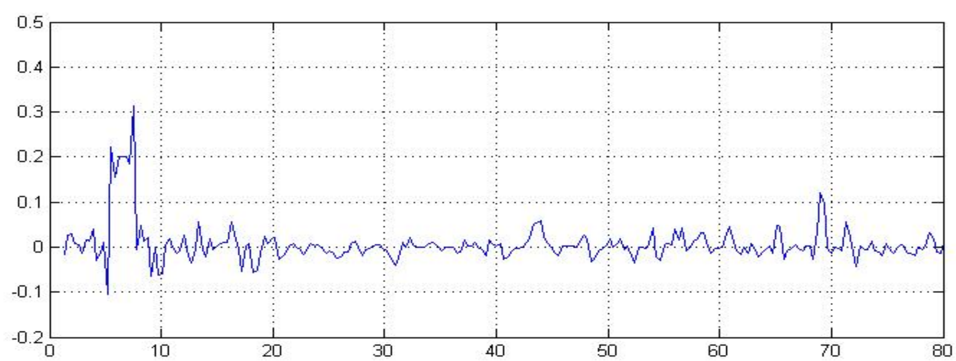

(c) Imaginary part of FRF

A2 Excitation frequency = 7.0 Hz

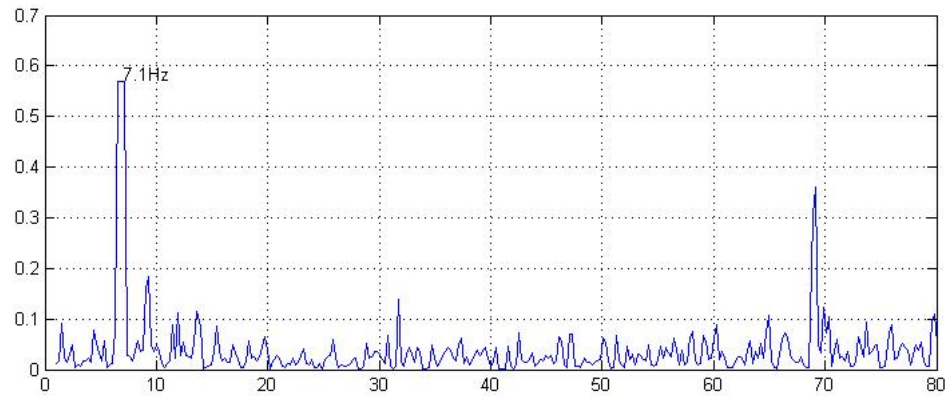

(a) Absolute value of FRF

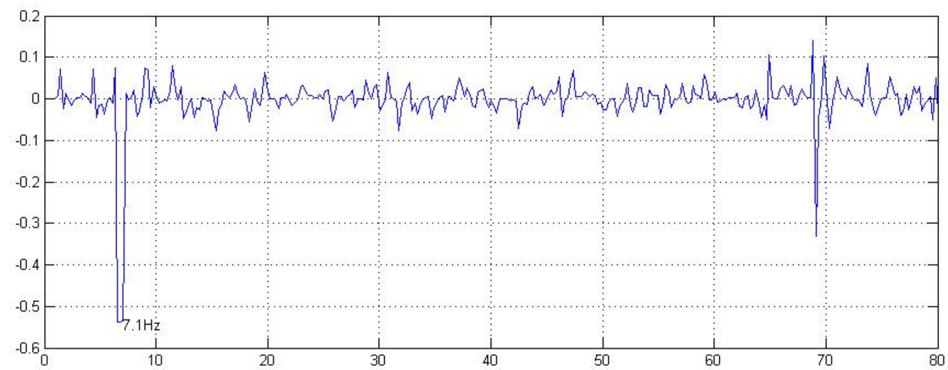

(b) Real part of FRF

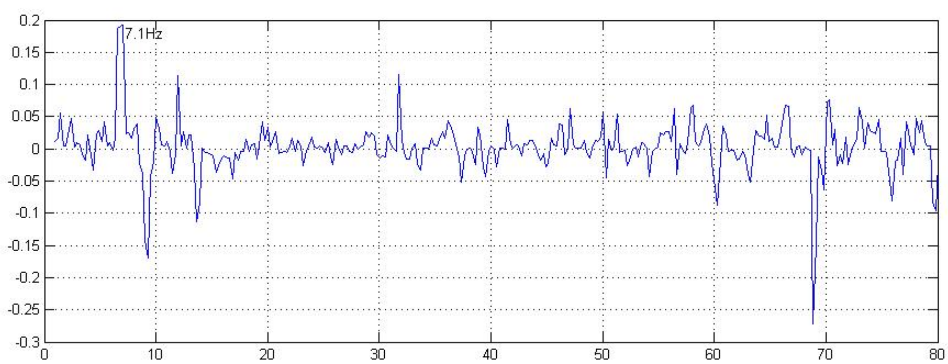

(c) Imaginary part of FRF

A3 Excitation frequency = 7.2 Hz

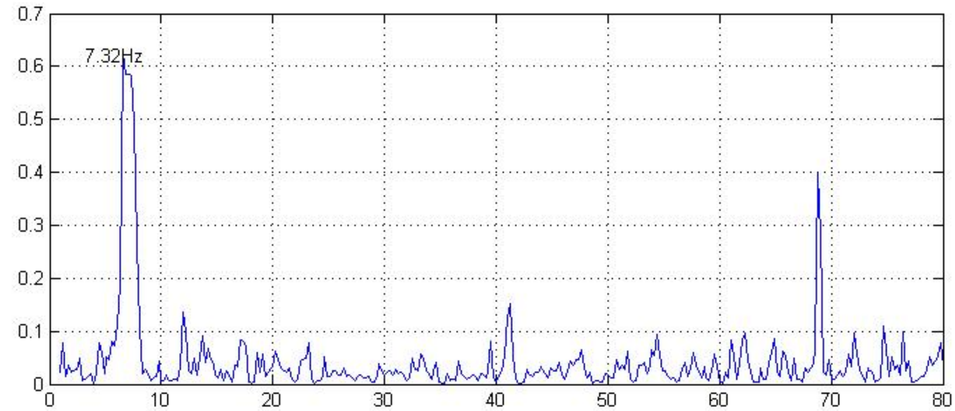

(a) Absolute value of FRF

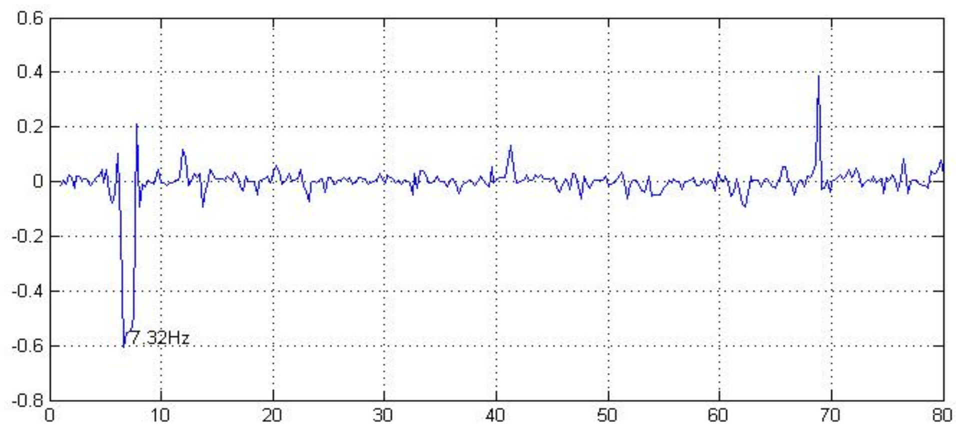

(b) Real part of FRF

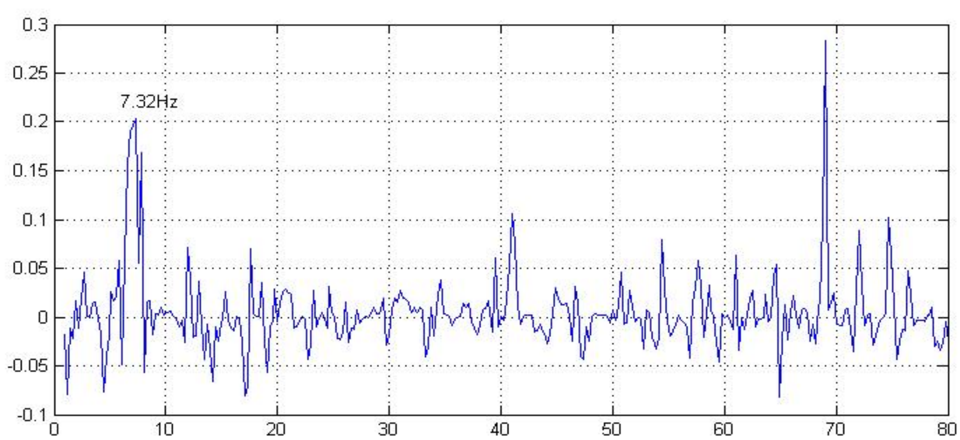

(c) Imaginary part of FRF

A4 Excitation frequency = 7.4 Hz

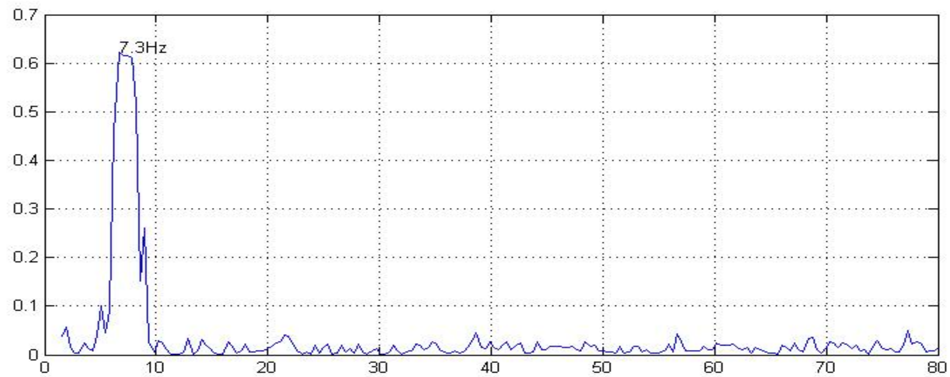

(a) Absolute value of FRF

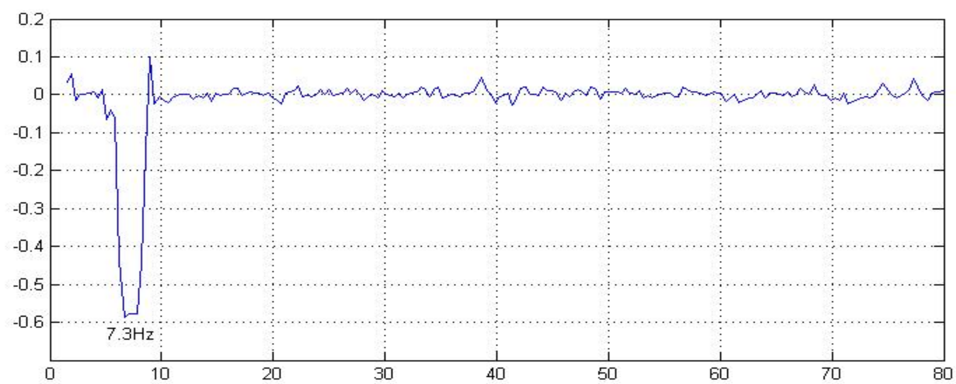

(b) Real part of FRF

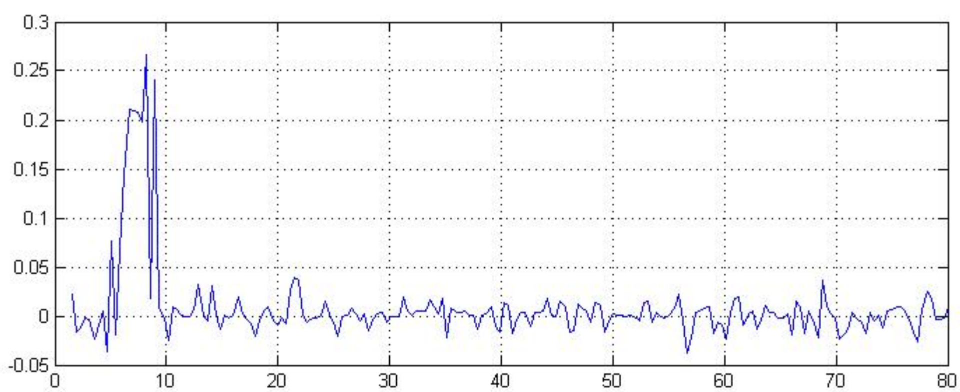

(c) Imaginary part of FRF

A5 Excitation frequency = 8.0 Hz

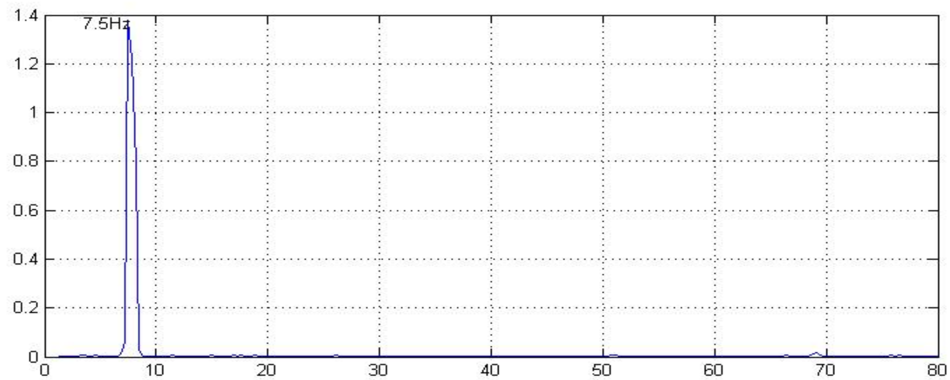

(a) Absolute value of FRF

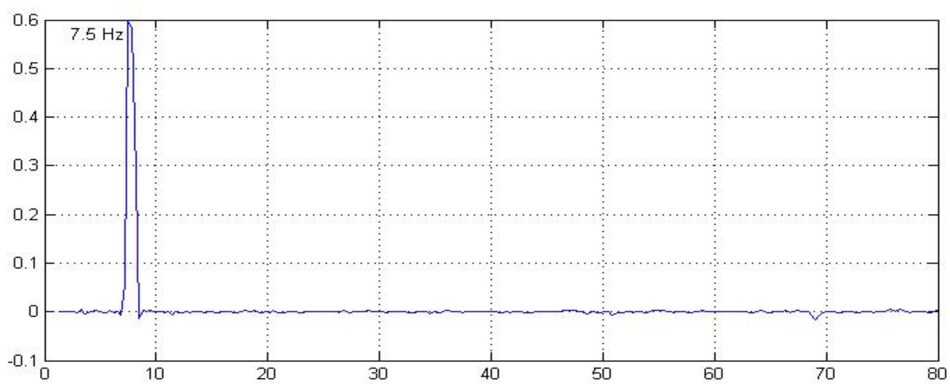

(b) Real part of FRF

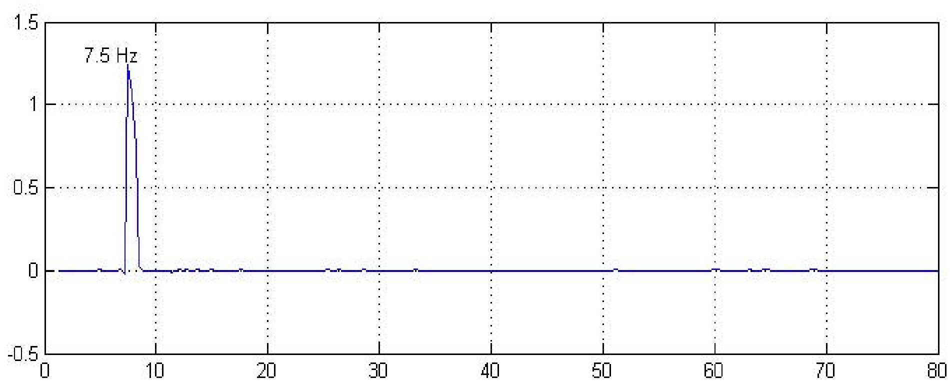

(c) Imaginary part of FRF